Cell Death Discovery

https://doi.org/10.1038/s41420-026-02961-y

Article in Press

Comparative phenotypic and molecular profiling of replicative and chemically-induced senescence in articular chondrocytes

Received: 1 August 2025

Revised: 27 November 2025

Accepted: 9 February 2026

Cite this article as: Arteaga, M.B., Tarasova, K., Kidtiwong, A. *et al.* Comparative phenotypic and molecular profiling of replicative and chemically-induced senescence in articular chondrocytes. *Cell Death Discov.* (2026). https://doi.org/10.1038/s41420-026-02961-y

Maria Belen Arteaga, Karyna Tarasova, Angkana Kidtiwong, Sinan Gültekin, Iris Gerner & Florien Jenner

Comparative Phenotypic and Molecular Profiling of Replicative and Chemically-Induced Senescence in Articular Chondrocytes

Running title: Comparative Analysis of Chondrocyte Senescence Models

Maria Belen Arteaga[1,*], Karyna Tarasova[1,*], Angkana Kidtiwong[1], Sinan Gültekin[1], Iris Gerner[1,2,+,] and Florien Jenner[1,2,+,#]

[1] University of Veterinary Medicine Vienna, Department for Small Animals and Horses, Centre for Equine Health and Research, Equine Surgery Unit, Veterinary Tissue Engineering and Regenerative Medicine Laboratory, Vienna, Austria

[2] Austrian Cluster for Tissue Regeneration

* shared first author

+ shared last author

corresponding author: florien.jenner@vetmeduni.ac.at

Abstract

Osteoarthritis (OA) is a degenerative joint disease characterized by the accumulation of senescent chondrocytes, which drive inflammation and cartilage degradation. However, in vitro models often fail to recapitulate the complexity of OA-associated senescence. This study compares three senescence induction strategies in chondrocytes—replicative senescence (HP), and stress-induced premature senescence (SIPS) via doxorubicin (DOX) and dexamethasone (DEX)—to establish a physiologically relevant in vitro model for OA research. To this end ovine chondrocytes (n=3) were subjected to serial passaging (to P40) or exposed to optimized concentrations of DOX (50 nM) or DEX (1 µM). Low passage (P3) cells served as controls. Cellular senescence was assessed via proliferation assays, cell cycle analysis, SA-β-gal activity, telomere length, ROS levels, mitochondrial function, transcriptomic profiling (NGS), and high-resolution mass spectrometry proteomic analysis

All models induced key senescence hallmarks including cell cycle and proliferation arrest, increased SA-β-gal activity, and mitochondrial dysfunction. HP cells showed telomere shortening, ROS accumulation, ATP depletion, and SASP secretion. DOX induced strong DNA damage responses and elevated apoptosis markers, while DEX induced senescence without significant ROS or apoptosis, suggesting distinct SIPS mechanisms. Transcriptomics revealed convergent downregulation of oxidative phosphorylation and selenoamino acid metabolism pathways, implicating mitochondrial dysfunction and redox imbalance as shared features. However, HP induced broad transcriptional suppression, also of inflammatory pathways, while

DOX and DEX activated immune and SASP-related pathways. Proteomics confirmed divergent secretory profiles, with DOX/DEX increasing SASP-factors and HP enriching matrix proteins.

In summary, although all models recapitulate fundamental aspects of senescence, they diverge in stress responses, immune signalling, and apoptosis profiles. HP most closely mimics aging-associated senescence, whereas DOX and DEX model distinct SIPS relevant to oxidative or pharmacological stress. These findings underscore the importance of model selection in senescence-focused OA research and highlight mitochondrial dysfunction as a central mechanistic hub across senescence pathways.

Keywords: Osteoarthritis, Aging, Chondrocytes, Dexamethasone, Doxorubicin, Replicative Senescence

Introduction

Osteoarthritis (OA), the most prevalent musculoskeletal disease, affects over 654 million individuals globally.[1–3] Characterized by progressive cartilage degeneration and articular inflammation, OA manifests clinically with pain, stiffness and limited mobility.[1–3] Despite its high prevalence and impact, effective curative treatments remain elusive, in part due to its clinical and molecular heterogeneity. Notably, osteoarthritic joints, regardless of the underlying molecular pathomechanisms (endotypes), consistently show increased levels of senescent cells, highlighting cellular senescence as a unifying pathological mechanism and a potential therapeutic target.

While chronological aging is the predominant risk factor for OA, articular cartilage also exhibits signs of premature aging, including cellular senescence, oxidative stress, and mitochondrial dysfunction, that both contribute to and reflect OA pathogenesis.[4–17] Indeed, OA joints exhibit an increased burden of senescent cells, and their presence correlates with disease severity.[4–17] Beyond their intrinsic dysfunction, senescent chondrocytes develop a senescence-associated secretory phenotype (SASP), characterized by hypersecretion of pro-inflammatory cytokines, matrix-degrading enzymes, and reactive oxygen species (ROS).[4–19] The SASP autocrinally and paracrinally reinforces senescence, promoting extracellular matrix breakdown and chronic inflammation, establishing a self-perpetuating cycle of senescence and inflammation that drives OA progression.[4–19] The causal role of senescent cells in OA is further supported by studies

showing that intra-articular transplantation of senescent chondrocytes induces OA-like changes, whereas their targeted clearance reduces disease burden.[9,15]

Chondrocyte senescence can arise from replicative mechanisms or stress-induced premature senescence (SIPS) due to extrinsic factors like oxidative stress, mechanical overload, or chronic inflammation.[4–19] The precise pathophysiological relevance of replicative senescence in OA remains debated, given the generally postmitotic and quiescent nature of articular chondrocytes and the uncertainty over whether in vivo cell turnover is sufficient to cause significant telomere erosion.[12,17,20–23] Nevertheless, during the early stages of OA, chondrocytes can re-enter the cell cycle and exhibit transient increases in proliferation and metabolic activity as part of a short-lived reparative response.[24,25] Consequently, cumulative replication over decades, particularly in the context of cartilage injury or articular inflammation, where mitotic activity may increase severalfold, could contribute to telomere attrition.[12,17,20–23] Although chondrocytes' telomeres shorten with age, suggesting a role for replicative aging in cartilage degeneration, the rate of erosion appears insufficient to fully account for the extent of chondrocyte senescence observed in OA. Thus, chondrocyte senescence in OA likely reflects the combined influence of lifelong replicative aging and accumulated damage from oxidative, mechanical and inflammatory stressors.[12,17,20–23]

Despite the recognized role of senescent cells in OA, traditional in vitro and in vivo models often fail to capture this dimension of disease pathophysiology.[26–29] While models based on

mechanical injury or cytokine stimulation can induce cartilage damage, inflammation, and SIPS under intense exposure, they typically do not account for pre-existing senescent cells.[26–29] Therefore, more physiologically relevant models incorporating senescent chondrocytes are crucial to better recapitulate the OA joint environment and support senescence-targeted research. In vitro, senescence can be induced either by serial passaging to model replicative senescence, or by exposure to noxious stimuli, such as oxidative stress or DNA-damaging agents, to induce SISP.[17,28,30–33] Among SISP inducers, doxorubicin (DOX), a chemotherapeutic drug, induces senescence via DNA double-strand breaks, topoisomerase-II inhibition, p53/p21 pathways activation, and ROS generation.[34–36] In chondrocytes, DOX exposure yields a stable senescent phenotype with cell-cycle arrest, increased SA-β-gal activity, altered morphology, and robust SASP secretion.[36] Dexamethasone (DEX), a potent glucocorticoid widely used for its anti-inflammatory and analgesic efficacy in OA treatment, exerts context-dependent effects, attenuating inflammation and pain in diseased cartilage, while inducing oxidative stress, matrix degradation, and senescence-like changes in healthy chondrocytes or under prolonged or high-dose exposure.[32,37–41] Thus, DOX and DEX serve as SISP models relevant for oxidative damage, DNA injury, or corticosteroid exposure in OA joints.

Given the central role of senescent cells in OA pathogenesis, this study compared three senescence induction methods: replicative senescence via prolonged serial passaging (HP) and chemically induced SISP via DOX and DEX with the aim to identify an in vitro model that reliably recapitulates the senescent phenotype characteristic of OA cartilage as a platform for mechanistic studies and the development of senescence-targeted therapies. We hypothesized

that while all senescence induction strategies converge on shared hallmarks, stressor-specific mechanisms diverge in ways that critically impact each model's fidelity for osteoarthritis research.

Materials and Methods

All experiments were carried out with 3 biological replicates. All experiments adhered to ethical guidelines and were performed with appropriate institutional approval (details: see declarations). For comprehensive descriptions of all experimental procedures, please refer to the Supplementary Material.

Chondrocyte isolation and culture

Primary ovine articular chondrocytes (n= 3 biological replicates), which had been previously isolated and biobanked from female, musculoskeletally mature Merino-cross sheep (2–5 years old, body weight 95 ± 12 kg) without orthopedic disease euthanized for reasons unrelated to this study,[42] were cultured in StemMACS® medium (Miltenyi Biotec, Cologne, Germany) supplemented with StemMACS® XF plus 1% Pen/Strep.

Senescence induction

Optimal doses and administration periods for doxorubicin (DOX) and dexamethasone (DEX) to induce senescence in chondrocytes were established through a pilot study. This preliminary work compared concentrations of 25, 50, 100, and 200 nM for DOX, and 1, 5, 10, and 20 µM for DEX (Supplementary Figure 1 and 2, Supplementary Results).[33,43,44] Based on cell viability and

gene expression levels of senescence-associated genes (Suppl. Results), a dose of 1 µM DEX and 50 nM DOX was selected for subsequent experiments. Cell seeding densities were adjusted to accommodate the varying durations of senescence induction for each protocol.

For DOX-induced senescence, cells in passage 3 (P3) were seeded at 9091 cells/cm² and treated with 50 nM DOX on days 1, 4, and 7 post-seeding. A recovery phase was initiated on day 10 by switching to DOX-free medium for 3 days.[43] For DEX-induced senescence, cells (P3) were seeded at 455 cells/cm^2 and treated with 1 µM every 72 hours over a total period of 9 days.[33,44] Replicative senescence (HP) was established by serial passaging of chondrocytes up to P40. Low passage cells (LP, P3) served as controls. Both LP and HP cells were seeded at 3030 cells/cm² for all assays.

Cell Cycle Analysis by Flow Cytometry

Cell cycle distribution was determined by propidium iodide (PI) staining. Cells were stained with a PI buffer containing sodium citrate, Triton X-100, RNase (Invitrogen, USA), and 20 µg/mL PI (Sigma-Aldrich, USA). Following a 30-minute incubation at 37°C, samples were analyzed using a flow cytometer, and data were processed using FlowJo (v10) with the Watson Pragmatic model.

Cell Viability and Proliferation Assays

Cell viability was quantitatively assessed using the MTT assay (Promega, USA). Absorbance was measured at 595 nm using a Varioskan LUX plate reader (Thermo Fisher, USA). Cell proliferation was continuously monitored by confluence measurements utilizing the IncuCyte® S3 live-cell analysis system (Sartorius, Germany).

Cell Morphology by Phalloidin Staining

Cells were fixed, permeabilized, and stained with Atto 488 Phalloidin (Sigma-Aldrich, USA) and DAPI (250 ng/mL). Images were acquired with the EVOS FL Auto microscope (Thermo Fisher) and quantified using ImageJ software (NIH, USA).

Relative Telomere Length by RT-qPCR

Genomic DNA was extracted using the DNeasy Blood & Tissue Kit (Qiagen, Germany). Telomere and single-copy gene (B2M) levels were quantified using EvaGreen® mix (Bio&Sell, Germany) on a ViiA7 qPCR system (Thermo Fisher, USA), and relative telomere length was calculated using the ΔΔCt method.

Immunofluorescence Staining

Cells were fixed, permeabilized, and blocked with buffer containing FCS, BSA, and Triton X-100. H3K9me3 was detected using rabbit anti-H3K9me3 (nsJ Bioreagents, USA) and Alexa Fluor 488 secondary antibody (Thermo Fisher). Samples were mounted with DAPI mounting medium (ibidi, Germany) and images acquired with a Zeiss Observer microscope.

SA-β-Gal Activity

Senescence-associated β-galactosidase activity was measured using a fluorometric assay kit (Cell Biolabs, USA) and the Varioskan LUX plate reader. Fluorescence was normalized to protein content, which was determined using the Qubit Protein Assay Kit (Thermo Fisher, USA).

Intracellular ROS Measurement

ROS levels were assessed using the OxiSelect™ ROS assay kit (Cell Biolabs, USA). Fluorescence was measured at 480/530 nm with the Varioskan LUX plate reader.

Enzyme-Linked Immunosorbent Assay (ELISA)

TNF-α concentrations in cell culture supernatants were measured using a sandwich ELISA kit (MBS2701341, MyBiosource, USA). Absorbance was recorded at 450 nm using the Varioskan LUX plate reader and normalized to protein content measured with Bradford assay (Bio-Rad, USA).

Caspase 3/7 Activity

Apoptotic activity was evaluated by measuring Caspase 3/7 activity using the Caspase-Glo® 3/7 Assay System (Promega, USA). Luminescence was measured using the Varioskan LUX plate reader and normalized to protein content measured with the Qubit Protein Assay Kit.

Gene Expression by RT-qPCR

RNA was extracted with TRIzol (Invitrogen, USA) and purified with chloroform and isopropanol precipitation. RT-qPCR was performed using the RevTrans EvaGreen One-Step kit (Bio&Sell, Germany), and gene expression was normalized to GAPDH and RPLP0.

Mitochondrial DNA Extraction and qPCR

Mitochondrial DNA was isolated using the DNeasy Blood & Tissue Kit (Qiagen, Germany), and qPCR was performed using EvaGreen qPCR Mix II (Bio&Sell, Germany) with specific primers for mitochondrial genes ND5, ND6, Cytb, and COX2.

Mitochondrial Staining and Flow Cytometry

Cells were stained with MitoTracker™ Green FM and TMRM or MitoSOX™ Red (Invitrogen, USA), and analyzed by flow cytometry (BD FACS Canto). DAPI (Thermo Fisher, USA) was used to stain dead cells.

ATP Quantification

Intracellular ATP levels were measured using the CellTiter-Glo® 2.0 Assay (Promega, USA). Luminescence was read with the Varioskan LUX plate reader and normalized to total protein measured with the Qubit assay.

Transcriptomic Analysis (3' RNA-Seq)

RNA-seq libraries were prepared using QuantSeq 3’ mRNA-Seq FWD protocol. Reads were mapped using STAR and analyzed with Bioconductor (DESeq2, IHW, EnhancedVolcano). Reference genomes were obtained from Ensembl and GENCODE.

Proteomics by Mass Spectrometry

Proteins from supernatants were digested using S-Trap microcolumns (Protifi), separated via nano-HPLC (Thermo), and analyzed on a Q-Exactive HF Orbitrap (Thermo Fisher). Data were processed using Proteome Discoverer and Perseus software.

Statistical analysis

Data (except NGS and Mass-Spec data) were analysed using Graphpad Prism (version 10.2.3). Statistical analysis was performed by paired t-test and paired one -way analysis of variance with

Dunnett's multiple comparison test. P-values < 0.05 were considered statistically significant. The variation within each group is presented in the form of standard error of the mean (SEM).

Results

Optimal senescence induction protocols for DOX, DEX, and HP cells were established in a pilot study (Suppl. Fig. 1 and 2, Suppl. Results).

Senescence Hallmarks

All three senescence induction methods led to cell growth arrest, each associated with a distinct cell cycle arrest phase (Fig. 1A). DOX -treated cells showed a significant decrease in G1 phase (p=0.0227), a non-significant accumulation in the S (p=0.3837) and a non-significant decrease in the G2 (p= 0.7515) phase compared to LP cells. DEX led to a non-significant accumulation of cells in the G1 (p=0.8071) phase, a significant decrease in the S phase (p=0.0057) and no change in the G2 (p>0.999) phase. HP cells showed non-significant decrease in the G1 phase (p=0.5716), a significant decrease in the S (p=0.0437) and non-significant decrease in the G2 phase (p=0.2911) (Fig. 1A). Cell proliferation was significantly impaired after 144h in DOX- (p=0.0076) and HP-treated cells (p=0.0339), while DEX showed a non-significant decrease (p=0.0880, Fig. 1B).

The ratio of cytoplasm area to nucleus area was significantly increased in DEX stimulated cells (DEX: p= 0.0129) and showed non-significant increases in DOX (p=0.0520) and HP cells (p=0.1736) (Fig. 1C-D).

All three methods also induced other key senescence hallmarks, including p21 gene expression, heterochromatin modifications, telomere attrition and SA-β-galactosidase activity. p21 gene expression was significantly upregulated in in DOX-stimulated chondrocytes (p=0.0004), with non-significant increases observed in DEX- (p=0.8291) and HP-treated cells (p= 0.7125, Figure 1E). H3K9me3 foci counts in positive cells significantly increased in DOX-stimulated chondrocytes (p=0.0044), with non-significant increases observed in DEX- (p=0.5284) and HP-treated cells (p=0.2459, Figure 1F, Supp. Fig. 3). Relative telomere length significantly decreased in HP chondrocytes (Primer A: p<0.0001; Primer B: p<0.0001) and DEX-stimulated cells (Primer B: p=0.0051), with a non-significant decrease in DOX-stimulated cells (Primer A: p=0.8181; Primer B: p=0.0051) (Figure 1G). SA-β-galactosidase activity significantly increased in DEX- (p=0.0373) and HP-treated cells (p=0.0009), showing a non-significant increase in DOX-treated cells (p=0.0696) (Figure 1H).

Oxidative stress and inflammatory markers showed model-specific patterns. Intracellular ROS levels significantly increased in DOX-treated (p=0.0046) and HP (p=0.0115) cells, but no alteration was observed in DEX-treated cells (p=0.9974, Fig. 1I). Similarly, TNF-α levels, a prominent SASP component, were significantly increased in DOX- (p<0.0001) and HP-treated cells (p<0.0001), but remained unaltered in DEX-treated cells (p=0.5232, Fig. 1J).

In contrast, apoptosis marker Caspase 3/7 activity was significantly increased only in DOX-treated cells (p=0.0051), with no significant change in DEX- (p=0.7598) or HP-treated cells (p=0.9844, Fig. 1K).

Mitochondrial function

Mitochondrial gene expression varied distinctly (Figure 2A). HP led to significant downregulation of ND5, ND6, Cytb (all $p<0.0001$), and COX-2 ($p=0.0003$). Conversely, DOX and DEX stimulation significantly upregulated ND5 (DOX: $p=0.0181$; DEX: $p=0.0490$), ND6 (DOX: $p=0.0031$; DEX: $p=0.0541$), and Cytb (DOX: $p=0.0296$; DEX: $p=0.0084$), though not COX-2 (DOX: $p=0.9855$; DEX: $p=0.8306$).

Mitochondrial membrane potential (TMRM) showed non-significant decreases across all groups (DEX: $p=0.4893$; DOX: $p=0.1472$; HP: $p=0.0658$, Figure 2B). Mitochondrial superoxide (MitoSOX) levels significantly increased in HP ($p<0.0001$) but significantly decreased in DEX-stimulated cells ($p=0.0435$), remaining unaltered in DOX-stimulated cells ($p=0.8545$). ATP significantly decreased in HP ($p=0.0006$) and DOX-stimulated chondrocytes ($p<0.0001$), but significantly increased with DEX treatment ($p=0.0279$, Figure 2C).

Next generation sequencing

Serial passaging induced the most extensive transcriptional remodeling, with 3,356 differentially expressed genes (DEGs) compared to LP (496 up, 2860 down, Figure 3A). DEX treatment yielded 538 DEGs (251 up, 287 down), while DOX yielded 651 DEGs (288 up, 363 down). A total of 136 DEGs were common across all three conditions. In addition, 192 DEGs were shared between HP and DOX, 116 between HP and DEX, and 115 between DOX and DEX (Figure 3B). Furthermore, unique DEGs were identified for each condition: 2912 for HP, 208 for DOX and 171 for DEX.

Canonical mitochondrial function and protein synthesis pathways, including “Oxidative Phosphorylation”, “Ribosomal Quality Control Signaling”, and “Selenoamino Acid Metabolism pathways, were consistently downregulated across all three models (Table 1, Figure 3C).

However, transcriptomic analysis also highlighted key divergences (Table 1, Supplementary Tables 1, 2, and 3, Figure 3C). HP and DOX-induced senescence strongly inhibited mitotic and cell cycle checkpoint signaling, including Cell Cycle Checkpoints pathway and Mitotic Metaphase and Anaphase. Conversely, DEX-treated cells showed activation of these pathways. These differences align with telomere erosion and DNA damage observed in HP and DOX, suggesting DEX induces a stress that doesn't immediately silence checkpoint genes.

Although p16 could not be directly detected, CDK4, a key target inhibited by p16 to enforce cell cycle arrest, was significantly downregulated in HP vs LP chondrocytes (logFC: –3.81; adj p = 0.0010), and non-significantly downregulated in DEX vs LP (logFC: –0.23; adj p = 0.94) and DOX vs LP (logFC: –0.58; adj p = 0.18). The observed suppression of CDK4 expression may indirectly suggest p16 pathway activation in the different senescence induction models. Additionally, CDKN2A (p16) interacting protein(CDKN2AIP), which regulates the DNA damage response by influencing pathways like the p53-HDM2-p21 pathway,[45] was upregulated in HP vs LP (logFC = 0.956; adj. p-value = 0.353), but not regulated in DEX vs LP (logFC = 0.012; adj. p-value = 1) and DOX vs LP (logFC = 0.081; adj. p-value = 1).

Furthermore, DEX and DOX activated pro-inflammatory and immune-activating programs, such as neutrophil degranulation and Class I MHC-mediated antigen processing and presentation, which were, conversely, inhibited in HP cells. This suggests that DEX and DOX-induced

senescence is driven by canonical SASP components with a more active immune signature, while HP-induced senescence presents a more attenuated immune profile (Table 3).

Proteomics

High-resolution mass spectrometry of the chondrocyte secretome identified 571 proteins, of which 185 were annotated and secreted (Suppl. Table 4).

Venn analysis of differently abundant proteins (DAPs) identified 155 DAPs (108 high, 47 low) between HP and LP chondrocytes, 154 DAPs (146 high, 8 low) between DEX vs LP and 104 (98 high, 6 low) DAPs between DOX vs LP (Fig. 4A).

A total of 64 DAPs were common across all three conditions. DEX and DOX shared more DAPs (32) than DEX and HP (30), while DOX and HP shared the fewest (4, Figure 4B). Furthermore, unique DAPs were identified for each condition: 57 for HP, 28 for DEX and 4 for DOX.

Proteomic analysis demonstrated functional distinctions (Figure 4C, Table 2, Supplementary Table 4). HP uniquely showed increased abundance of structural ECM proteins, including Tenascin-N, Fibulin-2, Cartilage oligomeric matrix protein (COMP), and Collagen XIV, alongside reduced Spondin-1 (SPON1). In contrast, in DEX and DOX key matrix components such as COMP were less abundant, and extracellular matrix glycoproteins like SPON1 were highly abundant, indicating potential impairment in matrix synthesis. Notably, several SASP factors (pentraxin-3, superoxide dismutase 3, EDIL3, IGF-binding protein 2) were less abundant in HP compared to LP cells, but highly abundant in DEX-treated cells and, to a lesser extent, in DOX-stimulated cells (Table 3).

Discussion

This study systematically compared three senescence induction methods - serial passaging (HP), doxorubicin (DOX), and dexamethasone (DEX) - to assess their biological fidelity and utility for modeling OA-associated chondrocyte senescence. All three protocols induced classical senescence features, albeit to varying extents. DOX and HP significantly reduced cellular proliferation, while DEX caused a non-significant decrease. DEX and HP significantly increased SA-β-Gal activity, whereas DOX induced a non-significant rise in SA-β-Gal activity. DOX significantly elevated H3K9me3 levels, while DEX and HP showed a non-significant increase. DEX significantly increased the cytoplasm-to-nucleus area ratio, with DOX and HP showing a non-significant trend. These findings indicate that each method activates distinct molecular pathways and stress responses, underscoring their differing relevance and applicability for senescence modeling and senotherapeutic research.

Mitochondrial dysfunction emerged as a converging hallmark across all models. Mitochondria play a central role in the regulation and execution of cellular senescence, serving as both the primary site of ATP production and the major source of ROS during oxidative phosphorylation (OXPHOS).[46–48] When mitochondrial function is compromised, this dual role shifts from supporting cellular energy demands to mediating oxidative damage.[46–48] Reflecting this functional disruption, transcriptomic analyses in this study revealed downregulation of gene sets involved in OXPHOS, electron transport, and Complex I biogenesis across all models, most

prominently in HP chondrocytes. However, the functional impact of mitochondrial impairment was model-specific. In both HP and DOX-treated cells, mitochondrial dysfunction coincided with elevated ROS, reduced ATP, and broad suppression of biosynthetic and proliferative pathways, including those governing DNA replication, cell cycle progression, ribosomal function, and translation. DEX produced a similar, though milder, transcriptomic profile. Intriguingly, DEX-treated chondrocytes paradoxically exhibited reduced mitochondrial superoxide, increased ATP levels, and upregulated mitochondrial gene expression. These findings may reflect a dose- and time-dependent compensatory metabolic adaptation, consistent with glucocorticoids' known cell type–specific and context-dependent effects on mitochondrial mass, metabolism and biogenesis via mitochondrial-localized glucocorticoid receptor signaling.[49–53] Such responses may transiently elevate ATP despite declining mitochondrial efficiency, particularly when biosynthetic demand is reduced due to senescence. DEX may also promote a shift from glycolysis to OXPHOS, contributing to altered metabolic profiles.[49–51]

All models also exhibited downregulation of the "Selenoamino Acid Metabolism" pathway, suggesting impaired antioxidant defense. Selenium and selenoproteins are essential for redox homeostasis, and their depletion accelerates senescence via increased ROS and SASP expression.[54–56] A ~72% proteomic overlap between selenium deficiency and senescence further supports this link,[54] suggesting that oxidative stress in all models is exacerbated by compromised redox buffering capacity.

Together, these findings underscore mitochondrial dysfunction and oxidative stress as core, reciprocally reinforcing hallmarks of cellular senescence, acting both as initiators and amplifiers of senescence across diverse stimuli. Aging and cellular stress promote mtDNA damage, which impairs electron transport, elevates ROS and activates p53/p21 signaling and SASP expression.[57] This feed-forward loop contributes to cellular dysfunction and OA progression. Notably, mitochondrial disturbances are exacerbated in the osteoarthritic joint, where mechanical stress and inflammation synergistically increase oxidative stress, which impairs matrix homeostasis, reduces proteoglycan synthesis, and disrupts antioxidant defenses.[2,4–8,10,58–61] Redox-sensitive pathways like NF-κB and PKCδ/IKKα/p53 further amplify MMP production and SASP release, linking oxidative stress to cartilage degradation.[2,4–8,10,58–61]

Despite these shared features, the three models differed in immune-related transcriptional and proteomic responses and cellular stress pathways. Notably, the neutrophil degranulation pathway was uniquely downregulated in HP chondrocytes, consistent with an immune-evasive phenotype that promotes age-related senescent cells accumulation despite a pro-inflammatory SASP.[62] In contrast, DOX and DEX induced SIPS, typically associated with active inflammatory signaling. Both maintained neutrophil degranulation-related gene expression, likely reflecting ongoing SASP activity, fueled by ROS and DNA damage responses, especially in DOX-treated cells. DOX is known to promote neutrophil-driven inflammation,[63] while glucocorticoids like DEX, despite their immunosuppressive effects, exert complex and contradictory actions on neutrophils, including enhanced survival and delayed apoptosis.[64]

DOX treatment triggered a robust DNA damage response (DDR), marked by increased p53, CDKN1A (p21), and H3K9me3 expression, consistent with its genotoxic mode of action.[31,34,36,65–68] Concurrent increases in ROS and SASP reinforced DDR-induced senescence. However, prominent activation of cleaved caspase-3/7 indicated early apoptosis, raising concerns about its fidelity as a model for chronic OA-associated senescence, where senescent chondrocytes typically are long-lived and resistant to apoptosis.[15] DOX-induced mitochondrial dysfunction likely contributed to this apoptotic priming via cytochrome c release, caspase activation and oxidative stress.[48,68,69] The overlap between senescence and apoptotic pathways could confound interpretations of SASP dynamics or senolytic efficacy.

In contrast, DEX-induced senescence developed more gradually and lacked strong DDR activation or apoptotic priming. Although DEX-stimulated chondrocytes exhibited classical senescence markers including SA-β-gal activity, cell cycle and proliferation arrest, SASP and altered morphology, they did not show elevated ROS. This supports a mechanistically distinct SIPS phenotype, consistent with clinical observations of glucocorticoid-induced cartilage degeneration and prior studies showing that DEX induces mitochondrial dysfunction and p53/p21 signaling independent of DNA damage.[33,52,53,70]

Serial passaging induced the most robust and consistent senescence phenotype, with marked reductions in mitochondrial gene expression and telomere length and increased ROS and SASP -

hallmarks of replicative senescence observed in aging and OA cartilage.[20,71] However, repeated trypsinization during passaging may introduce confounding stress. Trypsin-mediated detachment reduces intracellular glutathione levels and upregulates stress-response and apoptosis-related proteins, such as p53 and p21.[72–75] Proteomic studies have shown that trypsinisation decreases proteins associated with cell metabolism, growth, mitochondrial electron transportation and cell adhesion, while increasing proteins involved in cell apoptosis and cell cycle arrest.[72–75] This makes it critical to distinguish between replicative exhaustion and trypsin-induced damage when interpreting results from this model.

In summary, this study demonstrates that mitochondrial dysregulation is a central and unifying feature across diverse senescence models. While all models converged on core senescence hallmarks, they diverged in their molecular mechanisms, immune responses, and apoptotic profiles. These differences emphasize the need for careful model selection guided by mechanistic alignment with in vivo pathology, particularly for translational studies seeking to evaluate senotherapeutic strategies or dissect disease-specific senescence mechanisms.

Declarations

Ethics approval

No human or animal participants were involved in this study. Ovine chondrocytes had been obtained and biobanked from sheep euthanised for reasons unrelated to this study. Based on the "Good Scientific Practice. Ethics in Science und Research" regulation implemented at the University of Veterinary Medicine Vienna, the Institutional Ethics Committee (“Ethics and

Animal Welfare Committee") of the University of Veterinary Medicine Vienna does not require approval of in vitro cell culture studies, if the cells were isolated from tissue, which was obtained either solely for diagnostic or therapeutic purposes or in the course of institutionally and nationally approved experiments. The sheep from which the cells were obtained had been euthanised in the course of a study for which approval of the national ("Commission for Animal Research" of the Austrian Federal Ministry of Science, Research and Economy) and institutional ("Ethics and Animal Welfare Committee" of the University of Veterinary Medicine Vienna") animal welfare committees (ethical approval number: 68.205/0100-V/3b/2018, 13.7.2018) had been granted and which had been reported according to ARRIVE guidelines 2.0. Euthanasia had been conducted following sedation with detomidine and butorphanol, placement of a catheter in the jugular vein, and induction of general anesthesia with thiopental, by the administration of T61, a veterinary euthanasia drug containing tetracaine hydrochloride, mebezonium iodide, and embutramide.

All methods were carried out in accordance with the relevant guidelines and regulations.

Consent for publication

Not applicable

Availability of data and materials

The datasets generated and analysed during the current study are included in the paper and its supplementary materials. Please use the following link for the deposited RNA-Seq data: https://dataview.ncbi.nlm.nih.gov/object/PRJNA1347060?reviewer=cunkk64deujh7e6iggfprgkje0

Disclosure Statement

The authors declare that they have no competing interests

Funding

Funded by wings4innovation and the KHAN-I technology transfer fund.

Authors' contributions

M.B.A. K.T.: study design, data acquisition, analysis and interpretation, manuscript preparation; A.K., S.G..: data acquisition; I.G.: study design, data analysis and interpretation; F.J.: study conception and design, data analysis and interpretation, manuscript preparation. All authors reviewed the manuscript.

Acknowledgements

The authors acknowledge the Vetcore facility of the University of Veterinary Medicine Vienna, especially Dr. Ursula Reichart and Dr. Stephan Handschuh for their support with Imunofluorescence assays by Zeiss Observer. The authors acknowledge the use of ChatGPT (OpenAI) for linguistic refinement of the manuscript. All intellectual content, data interpretation, and conclusions remain the sole responsibility of the authors.

References

1 Cui A, Li H, Wang D, Zhong J, Chen Y, Lu H. Global, regional prevalence, incidence and risk factors of knee osteoarthritis in population-based studies. EClinicalMedicine 2020; 29: 100587.
2 Arra M, Abu-Amer Y. Cross-talk of inflammation and chondrocyte intracellular metabolism in osteoarthritis. Osteoarthr Cartil 2023; 31: 1012–1021.

3 Thomas E, Peat G, Croft P. Defining and mapping the person with osteoarthritis for population studies and public health. Rheumatology 2014; 53: 338–345.
4 Liu Y, Zhang Z, Li J, Chang B, Lin Q, Wang F et al. Piezo1 transforms mechanical stress into pro senescence signals and promotes osteoarthritis severity. Mech Ageing Dev 2023; 216: 111880.
5 Coryell PR, Diekman BO, Loeser RF. Mechanisms and therapeutic implications of cellular senescence in osteoarthritis. Nat Rev Rheumatol 2021; 17: 47–57.
6 Bolduc JA, Collins JA, Loeser RF. Reactive oxygen species, aging and articular cartilage homeostasis. Free Radic Biol Med 2019; 132: 73–82.
7 Mobasheri A, Matta C, Zákány R, Musumeci G. Chondrosenescence: Definition, hallmarks and potential role in the pathogenesis of osteoarthritis. Maturitas 2015; 80: 237–244.
8 Jiang W, Chen H, Lin Y, Cheng K, Zhou D, Chen R et al. Mechanical stress abnormalities promote chondrocyte senescence - The pathogenesis of knee osteoarthritis. Biomed Pharmacother 2023; 167: 115552.
9 Xu M, Bradley EW, Weivoda MM, Hwang SM, Pirtskhalava T, Decklever T et al. Transplanted Senescent Cells Induce an Osteoarthritis-Like Condition in Mice. J Gerontol Ser A: Biomed Sci Méd Sci 2017; 72: 780–785.
10 Minguzzi M, Cetrullo S, D'Adamo S, Silvestri Y, Flamigni F, Borzì RM. Emerging Players at the Intersection of Chondrocyte Loss of Maturational Arrest, Oxidative Stress, Senescence and Low-Grade Inflammation in Osteoarthritis. Oxidative Med Cell Longev 2018; 2018: 3075293.
11 Han Z, Wang K, Ding S, Zhang M. Cross-talk of inflammation and cellular senescence: a new insight into the occurrence and progression of osteoarthritis. Bone Res 2024; 12: 69.
12 Ramasamy TS, Yee YM, Khan IM. Chondrocyte Aging: The Molecular Determinants and Therapeutic Opportunities. Front Cell Dev Biol 2021; 9: 625497.
13 Vidal-Bralo L, Lopez-Golan Y, Mera-Varela A, Rego-Perez I, Horvath S, Zhang Y et al. Specific premature epigenetic aging of cartilage in osteoarthritis. Aging (Albany NY) 2016; 8: 2222–2230.
14 Harbo M, Delaisse JM, Kjaersgaard-Andersen P, Soerensen FB, Koelvraa S, Bendix L. The relationship between ultra-short telomeres, aging of articular cartilage and the development of human hip osteoarthritis. Mech Ageing Dev 2013; 134: 367–372.
15 Jeon OH, Kim C, Laberge R-M, Demaria M, Rathod S, Vasserot AP et al. Local clearance of senescent cells attenuates the development of post-traumatic osteoarthritis and creates a pro-regenerative environment. Nat Med 2017; 23: 775–781.
16 Jeon OH, David N, Campisi J, Elisseeff JH. Senescent cells and osteoarthritis: a painful connection. J Clin Investig 2018; 128: 1229–1237.
17 Martin JA, Buckwalter JA. Telomere Erosion and Senescence in Human Articular Cartilage Chondrocytes. J Gerontol Ser A: Biol Sci Méd Sci 2001; 56: B172–B179.
18 Ogrodnik M, Acosta JC, Adams PD, Fagagna F d'Adda di, Baker DJ, Bishop CL et al. Guidelines for minimal information on cellular senescence experimentation in vivo. Cell 2024; 187: 4150–4175.
19 Ajoolabady A, Pratico D, Bahijri S, Tuomilehto J, Uversky VN, Ren J. Hallmarks of cellular senescence: biology, mechanisms, regulations. Exp Mol Med 2025; : 1–10.
20 Rossiello F, Jurk D, Passos JF, Fagagna F d'Adda di. Telomere dysfunction in ageing and age-related diseases. Nat Cell Biol 2022; 24: 135–147.

21 Atasoy-Zeybek A, Hawse GP, Nagelli CV, Padilla CMLD, Abdel MP, Evans CH. Transcriptomic Changes During the Replicative Senescence of Human Articular Chondrocytes. Int J Mol Sci 2024; 25: 12130.
22 Fragkiadaki P, Nikitovic D, Kalliantasi K, Sarandi E, Thanasoula M, Stivaktakis PD et al. Telomere length and telomerase activity in osteoporosis and osteoarthritis. Exp Ther Med 2020; 19: 1626–1632.
23 Zhang X-X, He S-H, Liang X, Li W, Li T-F, Li D-F. Aging, Cell Senescence, the Pathogenesis and Targeted Therapies of Osteoarthritis. Front Pharmacol 2021; 12: 728100.
24 Goldring MB, Otero M, Tsuchimochi K, Ijiri K, Li Y. Defining the roles of inflammatory and anabolic cytokines in cartilage metabolism. Ann Rheum Dis 2008; 67: iii75.
25 Roach H, Aigner T, Soder S, Haag J, Welkerling H. Pathobiology of Osteoarthritis: Pathomechanisms and Potential Therapeutic Targets. Curr Drug Targets 2007; 8: 271–282.
26 Liu Y, Zhang Z, Li T, Xu H, Zhang H. Senescence in osteoarthritis: from mechanism to potential treatment. Arthritis Res Ther 2022; 24: 174.
27 Georget M, Defois A, Guiho R, Bon N, Allain S, Boyer C et al. Development of a DNA damage-induced senescence model in osteoarthritic chondrocytes. Aging (Albany NY) 2023; 15: 8576–8593.
28 Wang N, He Y, Liu S, Makarcyzk MJ, Lei G, Chang A et al. Engineering osteoarthritic cartilage model through differentiating senescent human mesenchymal stem cells for testing disease-modifying drugs. Sci China Life Sci 2022; 65: 309–327.
29 Jeon OH, David N, Campisi J, Elisseeff JH. Senescent cells and osteoarthritis: a painful connection. J Clin Investig 2018; 128: 1229–1237.
30 Hayflick L, Moorhead PS. The serial cultivation of human diploid cell strains. Exp Cell Res 1961; 25: 585–621.
31 Casella G, Munk R, Kim KM, Piao Y, De S, Abdelmohsen K et al. Transcriptome signature of cellular senescence. Nucleic Acids Res 2019; 47: 7294–7305.
32 Tarasova K, Arteaga MB, Kidtiwong A, Gueltekin S, Bileck A, Gerner C et al. Dexamethasone: a double-edged sword in the treatment of osteoarthritis. Sci Rep 2025; 15: 11832.
33 Poulsen RC, Watts AC, Murphy RJ, Snelling SJ, Carr AJ, Hulley PA. Glucocorticoids induce senescence in primary human tenocytes by inhibition of sirtuin 1 and activation of the p53/p21 pathway: in vivo and in vitro evidence. Ann Rheum Dis 2014; 73: 1405.
34 Bielak-Zmijewska A, Wnuk M, Przybylska D, Grabowska W, Lewinska A, Alster O et al. A comparison of replicative senescence and doxorubicin-induced premature senescence of vascular smooth muscle cells isolated from human aorta. Biogerontology 2014; 15: 47–64.
35 Hernandez-Segura A, Rubingh R, Demaria M. Identification of stable senescence-associated reference genes. Aging Cell 2019; 18: e12911.
36 Kirsch V, Ramge J-M, Schoppa A, Ignatius A, Riegger J. In Vitro Characterization of Doxorubicin-Mediated Stress-Induced Premature Senescence in Human Chondrocytes. Cells 2022; 11: 1106.
37 Black R, Grodzinsky A. DEXAMETHASONE: CHONDROPROTECTIVE CORTICOSTEROID OR CATABOLIC KILLER? Eur cells Mater 2019; 38: 246–263.
38 Sabatini FM, Cohen-Rosenblum A, Eason TB, Hannon CP, Mounce SD, Krueger CA et al. Incidence of Rapidly Progressive Osteoarthritis Following Intra-articular Hip Corticosteroid Injection: A Systematic Review and Meta-Analysis. Arthroplast Today 2023; 24: 101242.

39 McAlindon TE, LaValley MP, Harvey WF, Price LL, Driban JB, Zhang M et al. Effect of Intra-articular Triamcinolone vs Saline on Knee Cartilage Volume and Pain in Patients With Knee Osteoarthritis: A Randomized Clinical Trial. JAMA 2017; 317: 1967–1975.
40 Zeng C, Lane NE, Hunter DJ, Wei J, Choi HK, McAlindon TE et al. Intra-articular corticosteroids and the risk of knee osteoarthritis progression: results from the Osteoarthritis Initiative. Osteoarthr Cartil 2019; 27: 855–862.
41 Samuels J, Pillinger MH, Jevsevar D, Felson D, Simon LS. Critical appraisal of intra-articular glucocorticoid injections for symptomatic osteoarthritis of the knee. Osteoarthr Cartil 2021; 29: 8–16.
42 Ribitsch I, Bileck A, Egerbacher M, Gabner S, Mayer RL, Janker L et al. Fetal Immunomodulatory Environment Following Cartilage Injury—The Key to CARTILAGE Regeneration? Int J Mol Sci 2021; 22: 12969.
43 Wahlmueller M, Narzt M-S, Missfeldt K, Arminger V, Krasensky A, Lämmermann I et al. Establishment of In Vitro Models by Stress-Induced Premature Senescence for Characterizing the Stromal Vascular Niche in Human Adipose Tissue. Life 2022; 12: 1459.
44 Xue E, Zhang Y, Song B, Xiao J, Shi Z. Effect of autophagy induced by dexamethasone on senescence in chondrocytes. Mol Med Rep 2016; 14: 3037–3044.
45 Cao Y, Chen Z, Qin Z, Qian K, Liu T, Zhang Y. CDKN2AIP-induced cell senescence and apoptosis of testicular seminoma are associated with CARM1 and eIF4β. Acta Biochim Biophys Sin 2022; 54: 604–614.
46 Passos JF, Saretzki G, Ahmed S, Nelson G, Richter T, Peters H et al. Mitochondrial Dysfunction Accounts for the Stochastic Heterogeneity in Telomere-Dependent Senescence. PLoS Biol 2007; 5: e110.
47 Miwa S, Kashyap S, Chini E, Zglinicki T von. Mitochondrial dysfunction in cell senescence and aging. J Clin Investig 2022; 132: e158447.
48 Martini H, Passos JF. Cellular senescence: all roads lead to mitochondria. FEBS J 2023; 290: 1186–1202.
49 Hunter RG, Seligsohn M, Rubin TG, Griffiths BB, Ozdemir Y, Pfaff DW et al. Stress and corticosteroids regulate rat hippocampal mitochondrial DNA gene expression via the glucocorticoid receptor. Proc Natl Acad Sci 2016; 113: 9099–9104.
50 Aoki S, Morita M, Hirao T, Yamaguchi M, Shiratori R, Kikuya M et al. Shift in energy metabolism caused by glucocorticoids enhances the effect of cytotoxic anti-cancer drugs against acute lymphoblastic leukemia cells. Oncotarget 2017; 8: 94271–94285.
51 Weber K, Brück P, Mikes Z, Küpper J-H, Klingenspor M, Wiesner RJ. Glucocorticoid Hormone Stimulates Mitochondrial Biogenesis Specifically in Skeletal Muscle. Endocrinology 2002; 143: 177–184.
52 Luan G, Li G, Ma X, Jin Y, Hu N, Li J et al. Dexamethasone-Induced Mitochondrial Dysfunction and Insulin Resistance-Study in 3T3-L1 Adipocytes and Mitochondria Isolated from Mouse Liver. Molecules 2019; 24: 1982.
53 Graybeal K, Sanchez L, Zhang C, Stiles L, Zheng JJ. Characterizing the metabolic profile of dexamethasone treated human trabecular meshwork cells. Exp Eye Res 2022; 214: 108888.
54 Hammad G, Legrain Y, Touat-Hamici Z, Duhieu S, Cornu D, Bulteau A-L et al. Interplay between Selenium Levels and Replicative Senescence in WI-38 Human Fibroblasts: A Proteomic Approach. Antioxidants 2018; 7: 19.

55 Bjørklund G, Shanaida M, Lysiuk R, Antonyak H, Klishch I, Shanaida V et al. Selenium: An Antioxidant with a Critical Role in Anti-Aging. Molecules 2022; 27: 6613.
56 Lee MY, Ojeda-Britez S, Ehrbar D, Samwer A, Begley TJ, Melendez JA. Selenoproteins and the senescence-associated epitranscriptome. Exp Biol Med 2022; 247: 2090–2102.
57 Blanco FJ, Rego I, Ruiz-Romero C. The role of mitochondria in osteoarthritis. Nat Rev Rheumatol 2011; 7: 161–169.
58 Koike M, Nojiri H, Ozawa Y, Watanabe K, Muramatsu Y, Kaneko H et al. Mechanical overloading causes mitochondrial superoxide and SOD2 imbalance in chondrocytes resulting in cartilage degeneration. Sci Rep 2015; 5: 11722.
59 Toh WS, Brittberg M, Farr J, Foldager CB, Gomoll AH, Hui JHP et al. Cellular senescence in aging and osteoarthritis. Acta Orthopaedica 2016; 87: 6–14.
60 Diekman BO, Loeser RF. Aging and the emerging role of cellular senescence in osteoarthritis. Osteoarthr Cartil 2024; 32: 365–371.
61 Mobasheri A, Rayman MP, Gualillo O, Sellam J, Kraan P van der, Fearon U. The role of metabolism in the pathogenesis of osteoarthritis. Nat Rev Rheumatol 2017; 13: 302–311.
62 Iltis C, Moskalevska I, Debiesse A, Seguin L, Fissoun C, Cervera L et al. A ganglioside-based immune checkpoint enables senescent cells to evade immunosurveillance during aging. Nat Aging 2025; 5: 219–236.
63 Wang C, Kaur K, Xu C, Abu-Amer Y, Mbalaviele G. Chemotherapy activates inflammasomes to cause inflammation-associated bone loss. eLife 2024; 13: RP92885.
64 Ronchetti S, Ricci E, Migliorati G, Gentili M, Riccardi C. How Glucocorticoids Affect the Neutrophil Life. Int J Mol Sci 2018; 19: 4090.
65 Kozhukharova I, Zemelko V, Kovaleva Z, Alekseenko L, Lyublinskaya O, Nikolsky N. Therapeutic doses of doxorubicin induce premature senescence of human mesenchymal stem cells derived from menstrual blood, bone marrow and adipose tissue. Int J Hematol 2018; 107: 286–296.
66 Zhang X, Xiang S, Zhang Y, Liu S, Lei G, Hines S et al. In vitro study to identify ligand-independent function of estrogen receptor-α in suppressing DNA damage-induced chondrocyte senescence. FASEB J 2023; 37: e22746.
67 Gilliam LAA, Fisher-Wellman KH, Lin C-T, Maples JM, Cathey BL, Neufer PD. The anticancer agent doxorubicin disrupts mitochondrial energy metabolism and redox balance in skeletal muscle. Free Radic Biol Med 2013; 65: 988–996.
68 Ueno M, Kakinuma Y, Yuhki K, Murakoshi N, Iemitsu M, Miyauchi T et al. Doxorubicin Induces Apoptosis by Activation of Caspase-3 in Cultured Cardiomyocytes In Vitro and Rat Cardiac Ventricles In Vivo. J Pharmacol Sci 2006; 101: 151–158.
69 Kuznetsov AV, Margreiter R, Amberger A, Saks V, Grimm M. Changes in mitochondrial redox state, membrane potential and calcium precede mitochondrial dysfunction in doxorubicin-induced cell death. Biochim Biophys Acta (BBA) - Mol Cell Res 2011; 1813: 1144–1152.
70 Ma W, Brenmoehl J, Trakooljul N, Wimmers K, Murani E. Dexamethasone has profound influence on the energy metabolism of porcine blood leukocytes and prevents the LPS-induced glycolytic switch. Front Immunol 2025; 16: 1514061.
71 Vaiserman A, Krasnienkov D. Telomere Length as a Marker of Biological Age: State-of-the-Art, Open Issues, and Future Perspectives. Front Genet 2021; 11: 630186.

72 Huang H-L, Hsing H-W, Lai T-C, Chen Y-W, Lee T-R, Chan H-T et al. Trypsin-induced proteome alteration during cell subculture in mammalian cells. J Biomed Sci 2010; 17: 36.
73 Halliwell B. Oxidative stress in cell culture: an under-appreciated problem? FEBS Lett 2003; 540: 3–6.
74 Lordon B, Campion T, Gibot L, Gallot G. Impact of trypsin on cell cytoplasm during detachment of cells studied by terahertz sensing. Biophys J 2024; 123: 2476–2483.
75 Kurashina Y, Imashiro C, Hirano M, Kuribara T, Totani K, Ohnuma K et al. Enzyme-free release of adhered cells from standard culture dishes using intermittent ultrasonic traveling waves. Commun Biol 2019; 2: 393.

Figure Legends

Fig. 1: Effect of chemically induced senescence by Doxorubicin (DOX) and Dexamethasone (DEX) and serial passaging (HP) on chondrocytes (Senescence Hallmarks).

(A) DOX -treated cells showed a significant decrease in G1 phase (p=0.0227), a non-significant accumulation in the S (p=0.3837) and a non-significant decrease in the G2 (p= 0.7515) phase compared to LP cells. DEX led to a non-significant accumulation of cells in the G1 (p=0.8071) phase, a significant decrease in the S phase (p=0.0057) and no change in the G2 (p>0.999) phase. HP cells showed non-significant decrease in the G1 phase (p=0.5716), a significant decrease in the S (p=0.0437) and non-significant decrease in the G2 phase (p=0.2911).

(B) Cell proliferation after 144h in culture was significantly impaired in DOX stimulated (p= 0.0076) and in HP cells (p= 0.0339), while non-significant decreased in DEX (p= 0.0880) compared to LP chondrocytes.

(C) Phalloidin staining of F-actin (green) and Dapi of nucleus (blue). Typical fluorescence images show LP, HP, DEX and DOX stimulated cells (magnification 10X).

(D) The ratio cytoplasm area/ nucleus area was significantly increased in DEX stimulated cells (DEX: p= 0.0129) and non-significantly increased in DOX (p= 0.0520) and in HP (p= 0.1736) compared to LP cells.

(E) p21 gene expression was significantly upregulated in in DOX-stimulated chondrocytes (p=0.0004), with non-significant increases observed in DEX- (p=0.8291) and HP-treated cells (p= 0.7125).

(F) H3K9me foci counts in positive cells significantly increased in DOX stimulated chondrocytes ($p= 0.0044$) and non-significantly increased in DEX stimulated ($p= 0.5284$) and in HP cells ($p= 0.2459$) compared to LP chondrocytes.

(G) Telomere length significantly decreased in HP chondrocytes (Primer A: $p< 0.0001$, Primer B: $p< 0.0001$) and DEX (Primer A: $p= 0.1979$, Primer B: $p= 0.0051$) stimulated cells and decreased non-significantly in DOX (Primer A: $p= 0.8181$, Primer B: $p= 0.0051$) stimulated cells compared to LP chondrocytes

(H) SA-β Gal activity (Fluorescence/µg total protein concentration) significantly increased in DEX stimulated ($p=0.0373$) and HP ($p=0.0009$) cells and non-significantly increased DOX stimulated cells ($p=0.0696$) compared to LP chondrocytes.

(I) Intracellular reactive oxygen species (ROS) levels (concentration of DCF (nM)) significantly increased in DOX treated cells ($p=0.0046$) and in HP ($p=0.0115$), but no alteration was observed in DEX treated cells ($p=0.9974$) compared to LP cells.

(J) TNF-α levels (pg/mL/µg total protein concentration) were significantly increased in DOX treated cells ($p< 0.0001$) and in HP ($p< 0.0001$), but no alteration was observed in DEX treated cells ($p=0.5232$) compared to LP cells.

(K) Caspase 3/7 activity (Fluorescence/µg total protein concentration) was only significantly increased in DOX treated cells ($p=0.0051$) compared to LP cells, while no significant alteration was observed in DEX treated cells ($p=0.7598$) or in HP cells ($p=0.9844$) compared to LP cells.

n= 3 biological replicates with three to six technical replicates per donor per condition. Data shown as mean ± SEM. LP: Low Passage cells (P3); DEX: low passage cells (P3) stimulated with

DEX (1µM); DOX: low passage cells (P3) stimulated with DOX (50nM); HP: High Passage cells (P40). Not significant (ns, p≥0.05), *p<0.05, **p <0.01, ***p<0.001.

Fig. 2: Effect of chemically induced senescence by Doxorubicin (DOX) and Dexamethasone (DEX) and serial passaging (HP) on chondrocytes' mitochondrial function.

(A) Serial passaging led to significant downregulation of ND5 (p< 0.0001), ND6 (p< 0.0001), Cytb (p< 0.0001) and COX-2 (p= 0.0003) compared to LP chondrocytes, while DOX and DEX stimulation led to significant upregulation of ND5 (DOX: p= 0.0181 and DEX: p=0.0490), ND6 (DOX: p= 0.0031 and DEX: p= 0.0541), Cytob (DOX: p=0.0296 and DEX: p= 0.0084) but not COX-2 (DOX: p=0.9855 and DEX: p=0.8306) compared to LP chondrocytes.

(B) Mitochondrial membrane potential (TMRM) was non-significantly decreased in DEX (p= 0.4893) and DOX (p= 0.1472) stimulated cells and in HP cells (p= 0.0658) compared to LP cells (Fig. 2B). Mitochondrial superoxide (MitoSOX) levels were significantly increased in HP (p< 0.0001) and significant.ly decreased in DEX stimulated cells (p= 0.0435), while maintained unaltered in DOX stimulated cells (p= 0.8545) compared to LP cells

(C) ATP levels (Luminescence/µg total protein concentration) significantly decreased in HP chondrocytes (p= 0.0006) and in DOX stimulated cells (p< 0.0001), while significantly increased with DEX (p= 0.0279) compared to LP chondrocytes

n= 3 biological replicates with two to six technical replicates per donor per condition. Data shown as mean ± SEM. LP: Low Passage cells (P3); DEX: low passage cells (P3) stimulated with

DEX (1μM); DOX: low passage cells (P3) stimulated with DOX (50nM); HP: High Passage cells (P40). Not significant (ns, p≥0.05), *p<0.05, **p <0.01, ***p<0.001.

Fig. 3: Effect of chemically induced senescence by Doxorubicin (DOX) and Dexamethasone (DEX) and serial passaging (HP) on chondrocytes' gene expression (RNASeq analysis).

(A) Serial passaging of chondrocytes (HP) resulted in a total of 3,356 differentially expressed genes (DEGs) when compared to low-passage (LP) controls (496 up- and 2860 down-regulated). Chemical induction with DEX led to 538 DEGs (251 up- and 287 down-regulated), while DOX treatment yielded 651 DEGs (288 up- and 363 down-regulated).

(B) Venn diagram of the genes differentially regulated (adjusted p < 0.05) between HP vs LP, DEX vs LP and DOX vs LP comparisons groups showing a total of 136 DEGs were commonly affected across all three experimental conditions and the highest number of shared DEGs was observed between HP and DOX treatments, with 192 genes in common. DEX and HP shared 116 DEGs in total, while DEX and DOX stimulation shared 115 DEGs in total. Furthermore, 2912 unique DEGs were identified between HP vs LP chondrocytes, 171 unique DEGs in DEX vs LP and 208 unique DEGs between DOX vs LP.

(C) Heat map with canonical pathways enriched in genes differentially expressed in ovine adult articular chondrocytes between HP vs LP, DEX vs LP and DOX vs LP comparisons groups showing that all three senescence induction models (HP, DEX and DOX vs LP) activate of core senescence-associated pathways, but with distinct patterns reflecting their triggers. When comparing the top 20 Ingenuity Canonical Pathways shared across conditions, we observed a consistent

downregulation of pathways related to mitochondrial function and protein synthesis. Oxidative Phosphorylation (HP vs LP, z-score: 6.429; DEX vs LP, z-score: -2.333; DOX vs LP, z-score: -3), Ribosomal Quality Control Signaling Pathway (HP vs LP, z-score: -6.94; DEX vs LP, z-score: -3.024; DOX vs LP, z-score: -6.351) and Selenoamino acid metabolism (HP vs LP, z-score:-5.986; DEX vs LP, z-score: -5; DOX vs LP, z-score:-6.788) are suppressed in all three models. Both HP and DOX-induced senescence exhibited strong inhibition of mitotic and checkpoint-associated signaling, showed by the suppression of Cell Cycle Checkpoints pathway (HP vs LP, z-score: -6.47; DOX vs LP, z-score: -1.877) and Mitotic Metaphase and Anaphase (HP vs LP, z-score: -4.882; DOX vs LP, z-score: -2.4), whereas DEX-treated cells show activation of these same cell cycle progression pathways (DEX vs LP, z-score: 4.841; z-score: 5.692 respectively). DEX and DOX led to pathways like neutrophil degranulation (DEX, z-score: 2.082; DOX, z-score: 2.828) and Class I MHC mediated antigen processing and presentation (DEX, z-score: 2.2; DOX, z-score: 1.8) to be activated.

n= 3 biological replicates with one technical replicate per donor per condition. LP: Low Passage cells (P3); DEX: low passage cells (P3) stimulated with DEX (1µM); DOX: low passage cells (P3) stimulated with DOX (50nM); HP: High Passage cells (P40).

Fig. 4: Effect of chemically induced senescence by Doxorubicin (DOX) and Dexamethasone (DEX) and serial passaging (HP) on chondrocytes' proteomics.

(A) Serial passaging of chondrocytes (HP) resulted in 155 abundant DAPs (108 high and 47 low abundant) between HP and LP chondrocytes, 154 DAPs (146 high and 8 low abundant) between DEX vs LP and 104 (98 high and 6 low abundant) DAPs between DOX vs LP.

(B) Venn diagram of the differentially abundant proteins (adjusted $p < 0.05$) between HP vs LP, DEX vs LP and DOX vs LP comparisons groups showing that chemically induced and replicative induced cells shared 64 DAPs between each other. Chondrocytes stimulated with DEX shared more DAPs with DOX induced cells (32DAPs) than with HP cells (30 DAPs); in contrast DOX stimulated cells shared the least proteins with HP chondrocytes (4 DAPs). Furthermore, 57 unique DAPs were identified between HP vs LP chondrocytes, 28 unique DAPs DEX vs LP and 4 unique DAPs DOX vs LP.

(C) Heat map with top 10 low and high regulated proteins (ranked by Log_2 fold change) revealed that replicative senescence (HP) uniquely show a substantial increase in structural ECM proteins, including Tenascin-N (TNN, Log_2FC: 8.93), Fibulin-2 (FBLN2, Log_2FC: 7.61), Cartilage oligomeric matrix protein (COMP, Log_2FC: 5.82), and Collagen XIV (COL14A1, Log_2FC: 5.68); and the reduced expression of Spondin-1 (SPON1, Log_2FC: 1.65225). DEX and DOX stimulated cells do not exhibit this level of ECM protein induction; key matrix components such as COMP are less expressed (DEX Log FC: -1.45096; DOX Log FC: 6.3222) and extracellular matrix glycoproteins like SPON1 are highly expressed (DEX Log FC: 7.49653; DOX Log FC: -0.613366). Several secreted proteins associated with the SASP are strongly decreased in HP vs LP, including pentraxin-3 (PTX3 Log_2FC: -7.74642), the extracellular antioxidant enzyme superoxide dismutase 3 (SOD3 Log_2FC: -7.54732), an angiogenic glycoprotein (EDIL3 Log_2FC: -7.07963), and IGF-binding protein 2 (IGFBP2 Log_2FC: -6.11824). These same proteins are strongly highly expressed

in DEX-treated cells (PTX3 Log_2FC: 1.46653; SOD3 Log_2FC: 2.96889;EDIL3 Log_2FC: 1.88753 ; IGFBP2 Log_2FC: 1.98434) and to a lesser extent in the DOX condition (PTX3 Log_2FC: 0.299594 ; SOD3 Log_2FC: 1.73983; EDIL3 Log_2FC: 1.00945; IGFBP2 Log_2FC: 0.549595).

n= 3 biological replicates with one technical replicate per donor per condition. LP: Low Passage cells (P3); DEX: low passage cells (P3) stimulated with DEX (1µM); DOX: low passage cells (P3) stimulated with DOX (50nM); HP: High Passage cells (P40).

Table Legends

Table 1: Commonly or uniquely top 20 Ingenuity Canonical Pathways found among all sets of variables in Chondrocytes (sorted by descending absolute z-score).

Table 2: Commonly or uniquely top 10 up and down Differentially abundant Proteins found among all sets of variables in Chondrocytes.

Table 3: The senescence-associated secretory phenotype (SASP) factors found among all sets of variables in Chondrocytes.

Table 1: Commonly or uniquely top 20 Ingenuity Canonical Pathways found among all sets of variables in Chondrocytes (sorted by descending absolute z-score).

Comparable Set of Variables	Ingenuity Canonical Pathways	z-score HP vs LP	z-score Dexa vs LP	z-score Doxo vs LP
[HP vs LP]	Neutrophil degranulation	-7.553	2.082	2.828
	Protein Ubiquitination Pathway	-6.935	2.556	0.962

	Mitochondrial protein degradation	-6.252	-1.069	-2.496
	RHO GTPase cycle	-6.248	0.98	0.729
	Asparagine N-linked glycosylation	-6.112	0.905	1.508
	Class I MHC mediated antigen processing and presentation	-5.584	2.2	1.8
	Mitotic G2-G2/M phases	-5.5	2.449	-0.688
	Granzyme A Signaling	5.385	1.667	N/A
	Nuclear Cytoskeleton Signaling Pathway	-5.345	0.816	-0.688
[Dexa vs LP]	Mitotic Metaphase and Anaphase	-4.882	5.692	-2.4
	Mitotic Prometaphase	-4.16	5.604	-0.943
	RHO GTPases	-3.042	3.78	-2.138

	Activate Formins			
	Nucleosome assembly	-2.828	3.162	
	Protein Sorting Signaling Pathway	-3.883	3.051	2
	Regulation of mitotic cell cycle	-3.893	2.887	-2.121
	Synthesis of DNA	-4.523	2.887	-1.89
	Kinetochore Metaphase Signaling Pathway	-0.728	2.837	1.134
[Doxo vs LP]	Processing of Capped Intron-Containing Pre-mRNA	-4.21	-2.414	-5.154
	RNA Polymerase II Transcription	-4.258	-2.138	-4.025
	EIF2 Signaling	-3.938	-1.147	-3.656
	COPI-mediated anterograde transport	-3.773	1.941	3.606

	rRNA modification in the nucleus and cytosol	-5.209	-2.121	-3.162
	TP53 Regulates Transcription of DNA Repair Genes	-2.985	-1	-3
	tRNA Charging	-4	-2.646	-2.828
	Mitochondrial protein import	-3.9	0	-2.828
[HP vs LP] and [Doxo vs LP]	Mitochondrial translation	-7.211	-1.667	-3.317
	Oxidative Phosphorylation	-6.429	-2.333	-3
	SRP-dependent cotranslational protein targeting to membrane	-5.578	-2.646	-5.485
[Dexa vs LP] and [Doxo vs LP]	Eukaryotic Translation Elongation	-4.811	-4.69	-6.487
	Eukaryotic Translation Termination	-4.901	-4.583	-6.41

	Nonsense-Mediated Decay (NMD)	-4.906	-4.491	-6.223
	Eukaryotic Translation Initiation	-5.093	-4.041	-6.804
[HP vs LP] and [Dexa vs LP] and [Doxo vs LP]	Major pathway of rRNA processing in the nucleolus and cytosol	-8.433	-3.8	-7.147
	Ribosomal Quality Control	-6.94	-3.024	-6.351
	Signaling Pathway			
	Respiratory electron transport	-6.782	-3.162	-2.828
	Selenoamino acid metabolism	-5.986	-5	-6.788
	Response of EIF2AK4 (GCN2) to amino acid deficiency	-5.252	-4.796	-6.487
[HP vs LP] and	Cell Cycle Checkpoints	-6.47	4.841	-1.877

[Dexa vs LP]	Deubiquitination	-6.183	3.128	0.2
	Complex I biogenesis	-6.164	-3.317	-2.449

Table 2: Commonly or uniquely top 10 up and down Differentially abundant Proteins found among all sets of variables in Chondrocytes, sorted by descending logFC.

Comparable Set of Variables	Gene Symbol	LOG FC HP vs LP	LOG FC Dexa vs LP	LOG FC Doxo vs LP
[HP vs LP]	TNN	8.93487	0	1.28831
	FBLN2	7.60916	1.81018	2.17614
	LOC101111669	7.39552	0	2.0469
	CKB	6.60706	1.23089	1.03836
	COMP	5.82252	-1.45096	-0.613366
	PRDX5	5.69171	2.05213	2.52071
	COL14A1	5.67957	3.17315	1.51943
	SEC23A	5.51315	3.30076	3.40171

	LOXL2	-4.30531	-0.106401	-0.0519409
	COL5A1	-4.34614	1.07169	0.0837688
	DCN	-4.44267	0.820508	1.83648
	TNC	-4.7323	-0.101554	-0.784161
	CD109	-5.04904	1.83798	1.49548
	COL12A1	-5.89748	1.61587	0.00042851 8
	IGFBP2	-6.11824	1.98434	0.549595
	EDIL3	-7.07963	1.88753	1.00945
	SOD3	-7.54732	2.96889	1.73983
	PTX3	-7.74642	1.46653	0.299594
[Dex vs LP]	MAPK1	4.23177	3.74785	3.26995
	LGALS3	-2.55877	3.53249	3.31746
	MRC2	1.3605	0.58038	-0.218061
	PLOD2	3.26088	0.568567	0.00794792
	VTN	0.540558	-0.810243	-0.110742
	ENPP1	-0.829931	-1.0456	-0.26598
	CCDC80	-0.188419	-1.28869	0.772641
	POSTN	-2.27068	-1.85607	1.5701
[Dox vs LP]	RRBP1	4.61151	3.43837	4.85925

	ANGPTL5	-0.0987027	1.79267	3.81808
	QSOX1	-3.52953	1.12325	0.952967
	HSPG2	-1.5812	0.816158	0.914053
	GPC1	-3.65928	0.969566	0.814065
	COL16A1	-1.29796	2.47281	0.799962
	BGN	1.34528	-0.149156	-0.593702
	LOC114114921	-1.07612	0.772727	-1.15538
[Dex vs LP] and [Dox vs LP]	SPON1	1.65225	7.49653	6.3222
	PLCD1	1.16092	6.06344	6.8285
	HSPB1	1.9135	4.47272	4.00182
	FERMT2	0	4.02472	4.89491
	ARCN1	4.72982	4.00793	3.77874
	F13A1	-2.09206	3.60202	4.54532
	EMILIN1	1.35788	-0.348153	-0.804801
	LOC101102413	0.102794	-0.920633	-0.343047
	SERPINE1	-3.12593	-1.58794	-3.12957
	RBP4	-3.69731	-1.86536	-1.78199
	MVP	7.09993	6.40629	7.89294

[HP vs LP] and [Dex vs LP] and [Dox vs LP]	FUBP1	5.43331	4.65852	3.96437

	Gene expression/ Regulation						Protein abundance/ regulation					
Gene / Protein	Log FC	padj	Log FC	padj	Log FC	padj	Log FC	q-val	Log FC	q-val	Log FC	q-val

	name	CHP_LP	HPvsLP	CDEX_LP	DEXvsLP	CDOX_LP	DCXvsLP	CHP_LP	IHeHP_LP	CDEX_LP	IDeDEX_LP	CDOX_LP	IDeDOX_LP
...	interleukin 6(IL6)	-3.46	0.0028	-4.91	0.0000	-2.05	0.0014						

		22	48		90								
	interleukin 15(IL 15)	0.0.0.0.0.0.0.0	1.0.0.0.0.0.0.7	0.0.0.1.0.5.0.0	1.0.0.0.0.2.0.6	0.0.0.2.0.5.0.6	1.0.0.0.0.0.0.0						
	chemokine (C-X-C motif)	0.1.5.6.3	1.0.0.0.0	-0.0.0.2.4.5	1.0.0.0.0.0	-0.0.0.2.0.3	1.0.0.0.0						

	ligand 1 (melanoma growth stimulating activity, alpha)(C												

	XCL 1)												
	C-X-C motif chemokine ligand 8(CXCL8)	0.000000000	1.000000000	0.000000000	1.000000000	0.000250006	1.000000000						
	granulocyte-	0.3	1.0	-0.	1.0	0.0	1.0						

	macrophage colony-stimulating factor receptor subunit alph	1200	0020	0129	0030	2530	0000						

	a(LOC10111509)											
	complement C1s(C1S)	-4.7106	0.00800	-0.8793	0.01691	0.16927	0.6948	-1.9943	0.03832	2.3822	0.01399	1.9899	0.0215
	complement C3(L	0.001	1.000	-0.00	1.000	-0.00	1.000	-1.00	0.078	0.77	0.011	-1.11	0.04

	OC443475)	62	0.0	3.8.3	0.0	3.5.2	0.0	7.6.1	5.5	2.7	6.3	5.5.4	1.6
	vascular endothelial growth factor B(VEGFB)	0.2.5.9.9	0.0.6.1.2.0	0.1.5.2.0.3	1.0.0.0.0	0.0.1.0.0.7	1.0.0.0.0						

	vascular endothelial growth factor C(VEGFC)	-0.0834	1.000	-0.853	1.000	-0.170	0.703					
	vascular endo	0.0	1.0	0.0	1.0	0.0	1.0					

	theli al grow th facto r D(V EGF D)	0 0 0 0	0 0 0 0	2 6 7	0 0 0	3 9 6	0 0 0					
	epid erma l grow th facto	0 . 3 1 2 0	1 . 3 0 0 0	0 . 0 0 1 4	1 . 0 0 0 0	-0.000	1 . 0 0 0 0					

	r receptor(EGFR)					71						
	amphiregulin(AREG)	0.000000	1.000000	0.000000	1.000000	0.000255	1.000000					
	nerve growth	-1.3	1.00	-0.03	1.00	-0.03	1.00					

	factor(NGF)	422	020	154	000	092	000						
	insulin like growth factor binding protein 2(IG							-6.182	0.038	1.983	0.015	0.549	0.564

	FBP 2)												
	insulin like growth factor binding protein 3(IGFBP 3)	1.00400099	0.31430106	1.05060105	0.50001000								

	insulin like growth factor binding protein 4(IGFBP4)	0.156	1.0000	-0.0080	1.0000	-0.0203	1.0000	1.7262	0.7028	0.6648	0.2763	-0.3032	0.7636
	insulin like							-2	0.	0.	0.	0.	0.

	growth factor binding protein 5(IGFBP5)							.4970	0000	1516	4618	4131	6142
	insulin like growth	-6.0	0.00	-0.4	0.13	1.83	0.00	-1.8	0.06	1.41	0.03	1.18	0.09

	factor binding protein 6(IGFBP 6)	580	007	773	266	87	00	2665	93	04	15	22	60
	insulin like growth factor	-0.92	0.4167	-0.771	0.0416	0.187	0.831						

	binding protein 7(IGFBP 7)	27		61									
	hepatocyte growth factor(HGF)	-0.:34-74	0.6241	0.1961	1.0.1000	0.1.1206	1.0.000						

	angiogenin-1-like(LOC101113335)	-0.223300	1.000300	0.000000	-0.100800	1.000000						
	angiogenin-2-like(LOC101138696)	-0.837689	0.375800	0.000000	0.421010	1.000000						

	14959)												
	matrix metallopeptidase 1(MMP1)	-0.1389	1.00000	-0.08100	1.00000	1.00000							
	matrix metallope	-1.3	0.24	0.405	0.438	0.00	-1.00	0.001	2.00	0.001	1.70	0.01	

	ptidase 2(MMP2)	391	799	993	299	266	288	8359	935	037	006	893	889
	matrix metallopeptidase 13(MMP13)	0.000	1.000	0.004	1.000	0.000	1.000						

	TIMP metallopeptidase inhibitor 1(TIMP1)	-4.8544	0.00001	-0.9005	0.0039	0.1899	0.5103	-1.3775	0.0317	-0.2063	0.7851	0.3116	0.6553
	TIMP metallope	-1.4	0.013	-0.34	0.028	0.000	2.002	2.004	2.034	0.300	1.502	0.02

	ptidase inhibitor 2(TIMP2)	483	24	468	14	70	68	38	45	65	86	40	48
	TIMP metallopeptidase inhibitor	-7.2245	0.0000	0.0183	0.8073	0.1583	0.6610						

	3(TIMP3)											
	cathepsin B(CTSB)	-1.9834	0.0702	-0.1446	1.0003	0.1823	1.0000	-4.0543	0.0035	2.1710	0.0093	0.3703	0.6202
	cathepsin F(CTSF)	-1.27	0.24	-0.10	1.009	0.09	1.00						

		28	29	00	66	00						
	ADAM metallopeptidase with thrombospondin type 1	-5.28	0.00	-0.04	0.09	-0.03	0.90	-0.39	0.58	1.23	0.05	0.38	0.53

	motif 5(ADAMTS5)												
	plasminogen activator, tissue type(PLAT)	0.3120	1.0.0200	-0.0129	1.0.0000	-0.0071	1.0.0000						

	plasminogen activator, urokinase (PLAU)	-5.3510	0.000000	-1.2482	0.003760	-0.6560	0.0984						
	EGF containing fibulin	-4.002	0.00100	-1.880	0.00628	0.01858	0.0792	-0.03	0.88900	0.85210	0.09899	0.3196	0.0503

	extracellular matrix protein 1(EFEMP1)	66		14				47				
	lysyl oxidase like	-5.18	0.00	-1.08	0.00	-0.75	0.04	2.79	0.00	1.45	0.01	0.57	0.05

	3(LOXL3)	4.00	0.008	9.487	4.907	8.585	5.232	3.232	3.134	2.121	4.149	4.145
	periostin(POSTN)	-4.1142	0.0.0243	0.0.4267	1.0.4113	0.0.0741	-2.2707	0.0.0775	-1.8561	0.0.0199	1.0.5701	0.0.0822
	protein disulfide isomeras	-0.49	0.0.9163	0.0.4639	0.0.1628	0.0.0845	1.0.0648	0.0.0266	2.0.0414	0.0.0110	1.0.8304	0.0.0256

	e family A member 3(PDIA3)	76										
	quiescin sulfhydryl oxidase 1(QSOX1)	-0.372 5	1.0000	-0.873	1.0000	-0.805	1.0000	-3.295	0.043	1.133	0.233	0.930

	major vault protein(MVP)	-4.3029	0.01	0.03	0.06	0.03	0.33	0.70	0.64	0.01	0.78	0.01
	secreted frizzled related protein	0.74	0.40	0.05	0.20	0.30	0.10	0.85	0.37	0.03	0.23	0.07

	2(SFRP2)											
	inter-alpha-trypsin inhibitor heavy chain 2(ITIH2)						0.2357	0.1176	-0.2799	0.1460	-0.0296	0.8981

	ecto nucleotide pyrophosphatase/phosphodiesterase family mem	-1.378	0.216	-0.137	1.006	0.705	1.000						

	ber 5(ENPP5)												
.	intercellular adhesion molecule 1(ICAM1)	0.3107909	1.0.0.0.2	0.0.1.0.3	1.0.0.0.0	0.0.0.9.6	1.0.0.0.0						
.	plasmino	-2	0.0	-0.	1.0	-0.	1.0						

	gen activator, uroki nase recep tor(PLA UR)	.14365	0.16159	0.00308	.0089	0.0000						
	Fas cell surface death	-1.73	0.0.0972871	0.0.4236162	0.0.7410	0.0.2100						

	receptor(FAS)	00											
	thrombospondin 1(THBS1)	-0.1800	1.0000	0.2620	0.4074	0.2910	0.4222	0.3719	0.0717	1.6400	0.0422	2.2760	0.0203
	thrombospondin							3.95	0.00	2.05	0.04	1.26	0.01

	2(THBS2)						07	37	58	32	22	80
	serpin family E member 1(SERPINE1)	-2.5859	0.0253	-0.3581	0.8542	-0.659	0.1967	-3.1259	0.0000	-1.5879	0.0233	-3.1296	0.0255
	serpin family B	-4.5	0.001	0.031	0.25	1.289	0.00	-3.5	0.000	2.009	0.002	3.592	0.02

	member 1(SERPINB1)	161	015	255	356	260	000	0916	9906	0256	2551	011
	serpin family F member 1(SERPINF1)	-2.3370	0.04150	-1.1553	0.0311	-0.8898	0.0429	3.30495	0.00900	0.25900	0.48655	-0.26222	0.4433

	serpin family G member 1(SERPING1)	-2.3458	0.03488	-0.1682	1.00070	0.00474	1.00000	-3.1116	0.05103	2.32033	0.01441	0.08646	0.1079
	S100P binding protein	-0.51	1.000	-0.14	1.000	-0.12	1.00						

	in(S100P BP)	37	0.01	0.07	20	0.00						
	S100 calcium binding protein B(S100B)	0.42297	0.0.5578	0.4.710	1.0.406	0.4.920	1.0.00					
	S100 calcium	-6.0	0.0.08	0.0.8	-1.0	0.0.0	-0.1	0.1.6	0.0.0	1.3.0	0.0.0	

	binding protein A4(S100A4)	1516	0010	0012	4666	0843	1061	7606	1907	9233	1900	2155	4055
	HtrA serine peptidase 1(HTRA1)	-3.0685	0.0096	-0.137	1.00708	0.2578	0.5713	1.8632	0.6042	1.6023	0.0104	1.2353	0.0628

	secreted protein acidic and cysteine rich(SPARC)	-2.6339	0.0.00000	-0.0.2060	0.0.4747	1.0.4207	0.0.0202	1.0.1569	0.0.1887	1.0.4187	0.0.0152	1.0.4303	0.0.0382
	proteasome	-6.0	0.0.09	0.0.04	0.0.04	0.0.00	1.0.09	0.0.04	1.0.04	0.0.00	1.0.02	0.0.00

	20S subunit alpha 7(PSMA7)	3170	0202	0208	0038	8749	2196	0966	6866	2060	8366	4122	
	proteasome 20S subunit beta	-2.5862	0.0000	-0.3453	0.2514	-0.3409	0.3424						

	4(PSMB4)											
	follistatin like 1(FSTL1)	0.1174	1.00400	-0.0089	0.06829	0.0799	0.08191	0.08306	1.05800	0.01600	0.1842	0.7689
	cystatin C(CST3)	-5.64	0.00	-0.57	0.038	0.032	0.041	-3.28	0.00	1.701	0.00	1.54	0.04

		86	00	04	51	42	53	59	36	15	98	99	13
	cellular communication network factor 2(CCN2)	-1.9736	0.0006	-1.8771	0.0000	-0.7820	0.0140	-0.7490	0.0303	-0.2718	0.6775	0.0981	0.8347

	cadherin 13(CDH13)	-4.60227	0.0001	-0.60045	0.03244	-0.4972	0.12667	-1.7728	0.0977	1.7785	0.0103	1.3416	0.026
	clusterin(LOC101113728)	-6.55598	0.0000	-1.0080	0.0063	0.7473	0.0188	2.7319	0.0140	0.0000	1.0000	0.0000	1.0000

	pentraxin 3(PTX3)	-3.6839	0.2.0.0.3.4	0.5.6.0.0.8	0.3.5.6.0.0.7	0.0.0.0.0.0	-7.7.4.6.4	0.1.0.0.2.3	1.4.6.6.5	0.0.2.6.0	0.0.2.9.9.6	0.6.9.8.5
	dipeptidyl peptidase 4(DPP4)	0.0.0.6.0.0.0	0.3.8.7.6.0.3	0.0.9.5.1.0.7	3.0.6.0.5.5	0.0.0.5						
	laminin	-2	0.0.0.0.0									

	subunit beta 1(LAMB1)	.8349	0122	3033	6529	4465	2339						
	fibronectin 1(FN1)	-2.8517	0.0041	-0.1548	0.5666	0.1908	0.6397	-9.1643	0.0071	-0.4861	0.1470	-0.0889	0.5100
	HMG box	0.	0.	0.	1.	-0	1.						

	domain-containing protein (W5NY72_SHEEP)	74494	44823	10305	.2051	00							
	high mobility	-1.	0.29	0.0	-0.	0.6							

	group box 2(HMGB 2)	4367	6940	6808	4401	2009	3708						
	high mobility group box 3(HMGB 3)	-1.3985	0.1715	0.5228	0.4844	-0.3261	0.7019						

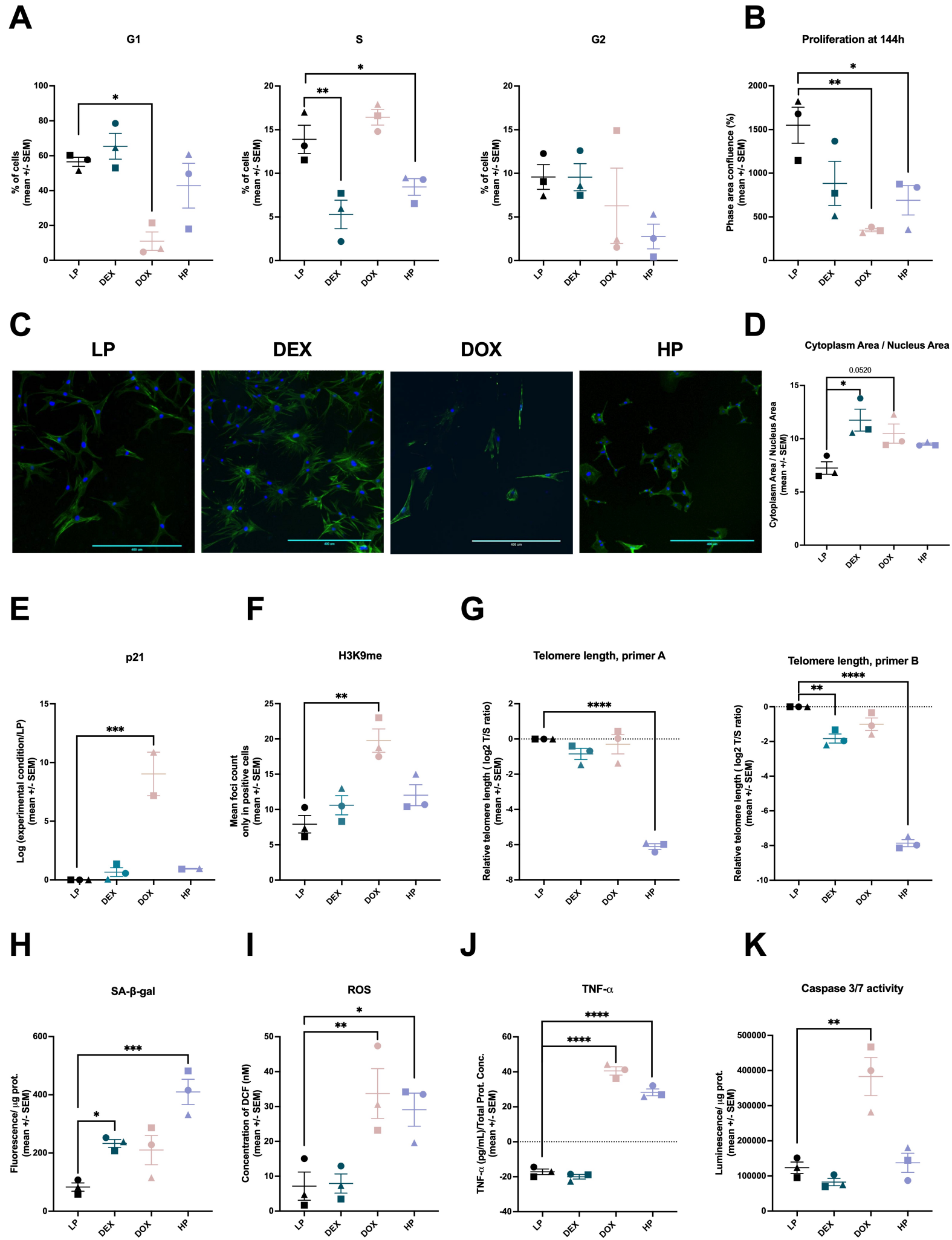
A
G1
S
G2
% of cells (mean +/- SEM)
LP
DEX
DOX
HP
B
Proliferation at 144h
Phase area confluence (%) (mean +/- SEM)
C
LP
DEX
DOX
HP
D
Cytoplasm Area / Nucleus Area
0.0520
Cytoplasm Area / Nucleus Area (mean +/- SEM)
E
p21
Log (experimental condition/LP) (mean +/- SEM)
F
H3K9me
Mean foci count only in positive cells (mean +/- SEM)
G
Telomere length, primer A
Relative telomere length (log2 T/S ratio) (mean +/- SEM)
Telomere length, primer B
H
SA-β-gal
Fluorescence/ µg prot. (mean +/- SEM)
I
ROS
Concentration of DCF (nM) (mean +/- SEM)
J
TNF-α
TNF-α (pg/mL)/Total Prot. Conc. (mean +/- SEM)
K
Caspase 3/7 activity
Luminescence/ µg prot. (mean +/- SEM)

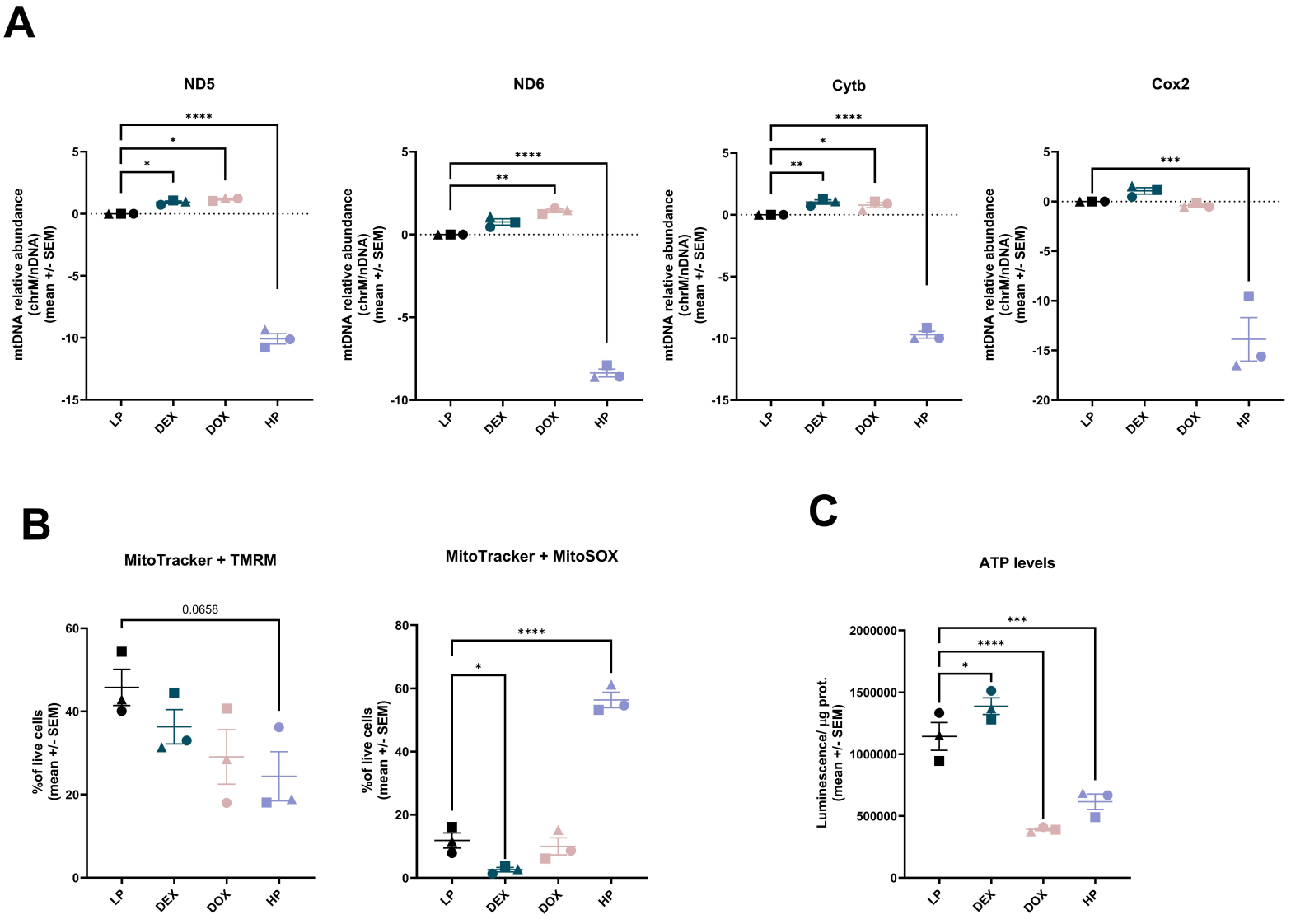
A
ND5
ND6
Cytb
Cox2
mtDNA relative abundance (chrM/nDNA) (mean +/- SEM)
LP
DEX
DOX
HP
B
MitoTracker + TMRM
0.0658
%of live cells (mean +/- SEM)
MitoTracker + MitoSOX
C
ATP levels
Luminescence/ µg prot. (mean +/- SEM)

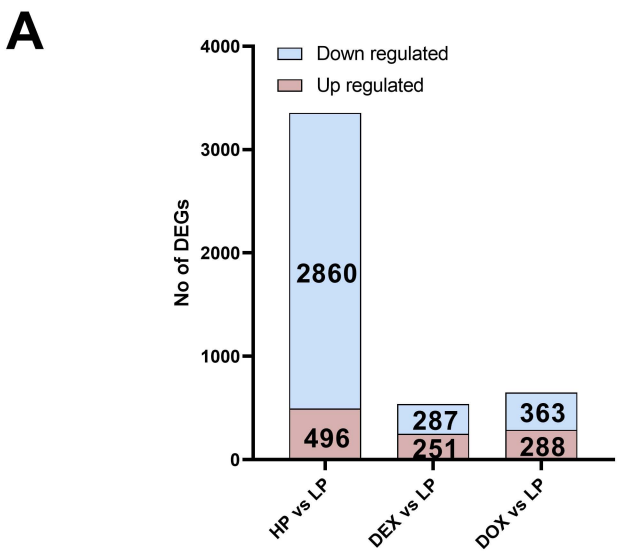
A
Down regulated
Up regulated
No of DEGs
4000
3000
2000
1000
0
2860
496
287
251
363
288
HP vs LP
DEX vs LP
DOX vs LP

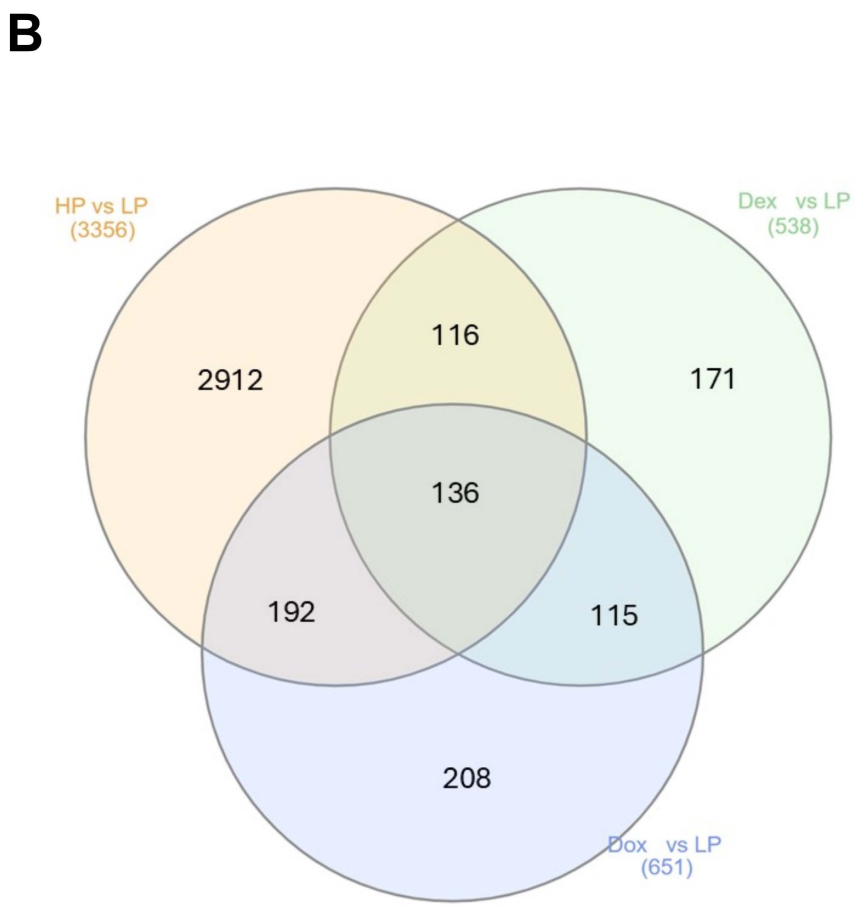
B
HP vs LP
(3356)
Dex vs LP
(538)
Dox vs LP
(651)
2912
116
171
136
192
115
208

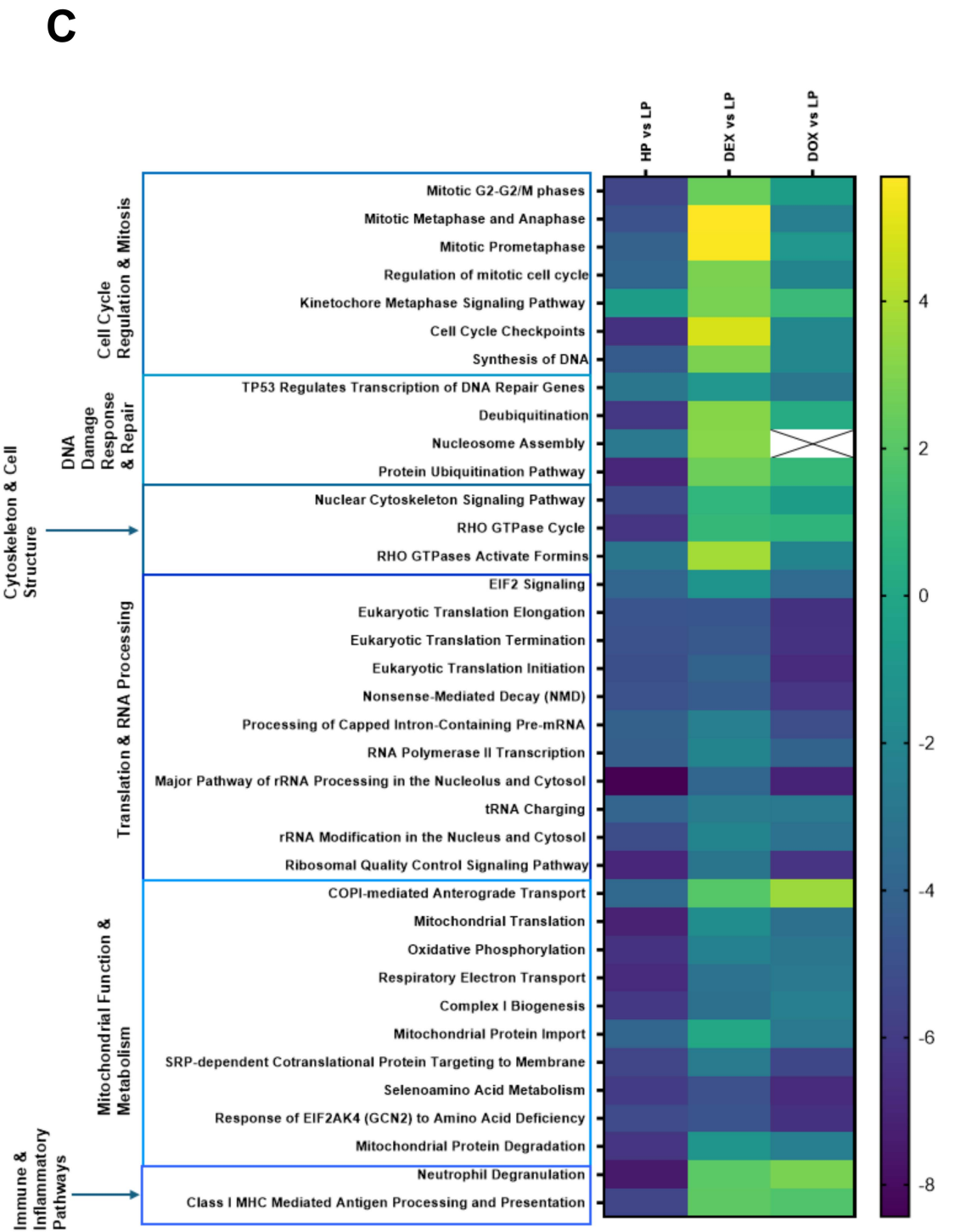
C
HP vs LP
DEX vs LP
DOX vs LP
Cell Cycle Regulation & Mitosis
Mitotic G2-G2/M phases
Mitotic Metaphase and Anaphase
Mitotic Prometaphase
Regulation of mitotic cell cycle
Kinetochore Metaphase Signaling Pathway
Cell Cycle Checkpoints
Synthesis of DNA
DNA Damage Response & Repair
TP53 Regulates Transcription of DNA Repair Genes
Deubiquitination
Nucleosome Assembly
Protein Ubiquitination Pathway
Cytoskeleton & Cell Structure
Nuclear Cytoskeleton Signaling Pathway
RHO GTPase Cycle
RHO GTPases Activate Formins
Translation & RNA Processing
EIF2 Signaling
Eukaryotic Translation Elongation
Eukaryotic Translation Termination
Eukaryotic Translation Initiation
Nonsense-Mediated Decay (NMD)
Processing of Capped Intron-Containing Pre-mRNA
RNA Polymerase II Transcription
Major Pathway of rRNA Processing in the Nucleolus and Cytosol
tRNA Charging
rRNA Modification in the Nucleus and Cytosol
Ribosomal Quality Control Signaling Pathway
Mitochondrial Function & Metabolism
COPI-mediated Anterograde Transport
Mitochondrial Translation
Oxidative Phosphorylation
Respiratory Electron Transport
Complex I Biogenesis
Mitochondrial Protein Import
SRP-dependent Cotranslational Protein Targeting to Membrane
Selenoamino Acid Metabolism
Response of EIF2AK4 (GCN2) to Amino Acid Deficiency
Mitochondrial Protein Degradation
Immune & Inflammatory Pathways
Neutrophil Degranulation
Class I MHC Mediated Antigen Processing and Presentation
4
2
0
-2
-4
-6
-8

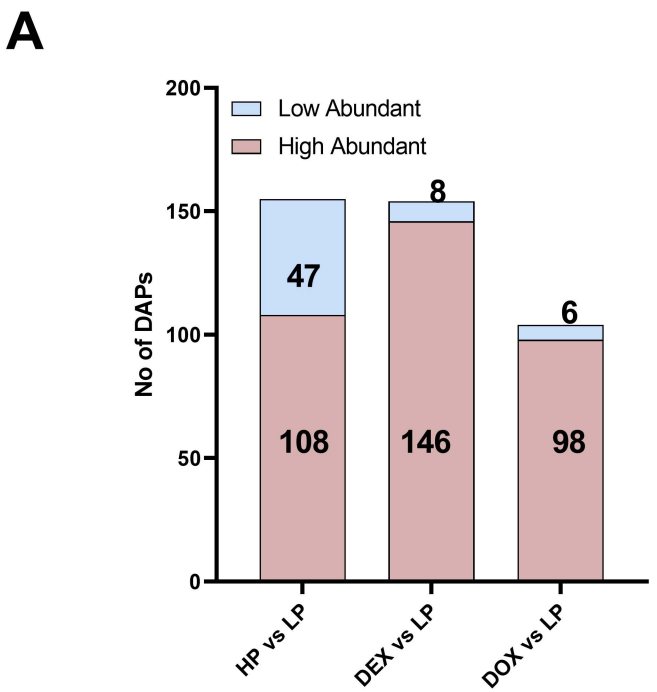
A
Low Abundant
High Abundant
No of DAPs
200
150
100
50
0
47
108
8
146
6
98
HP vs LP
DEX vs LP
DOX vs LP

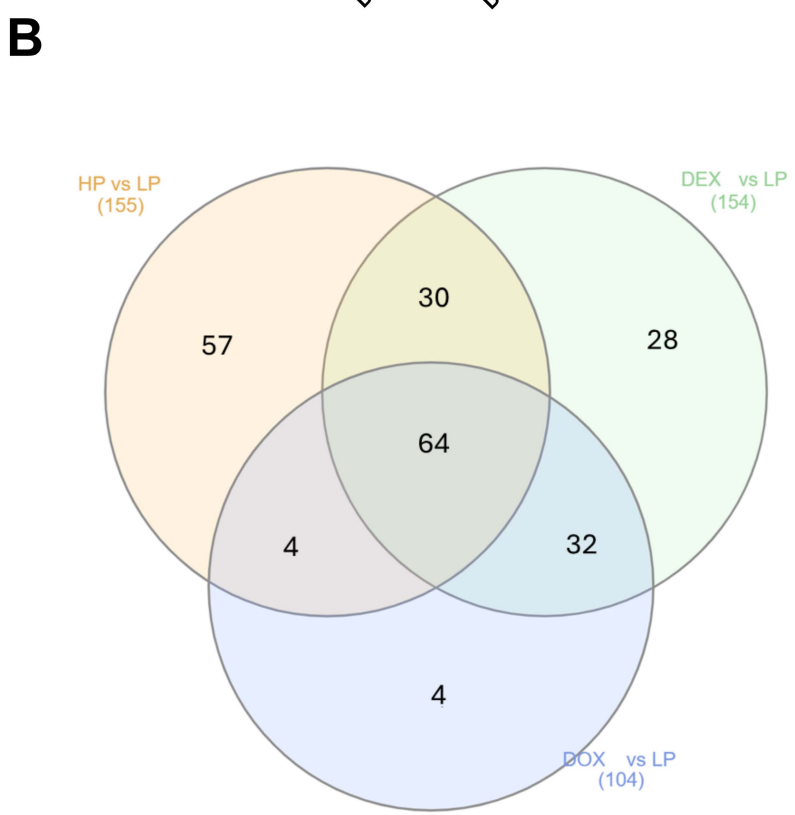
B
HP vs LP
(155)
DEX vs LP
(154)
DOX vs LP
(104)
57
30
28
64
4
32
4

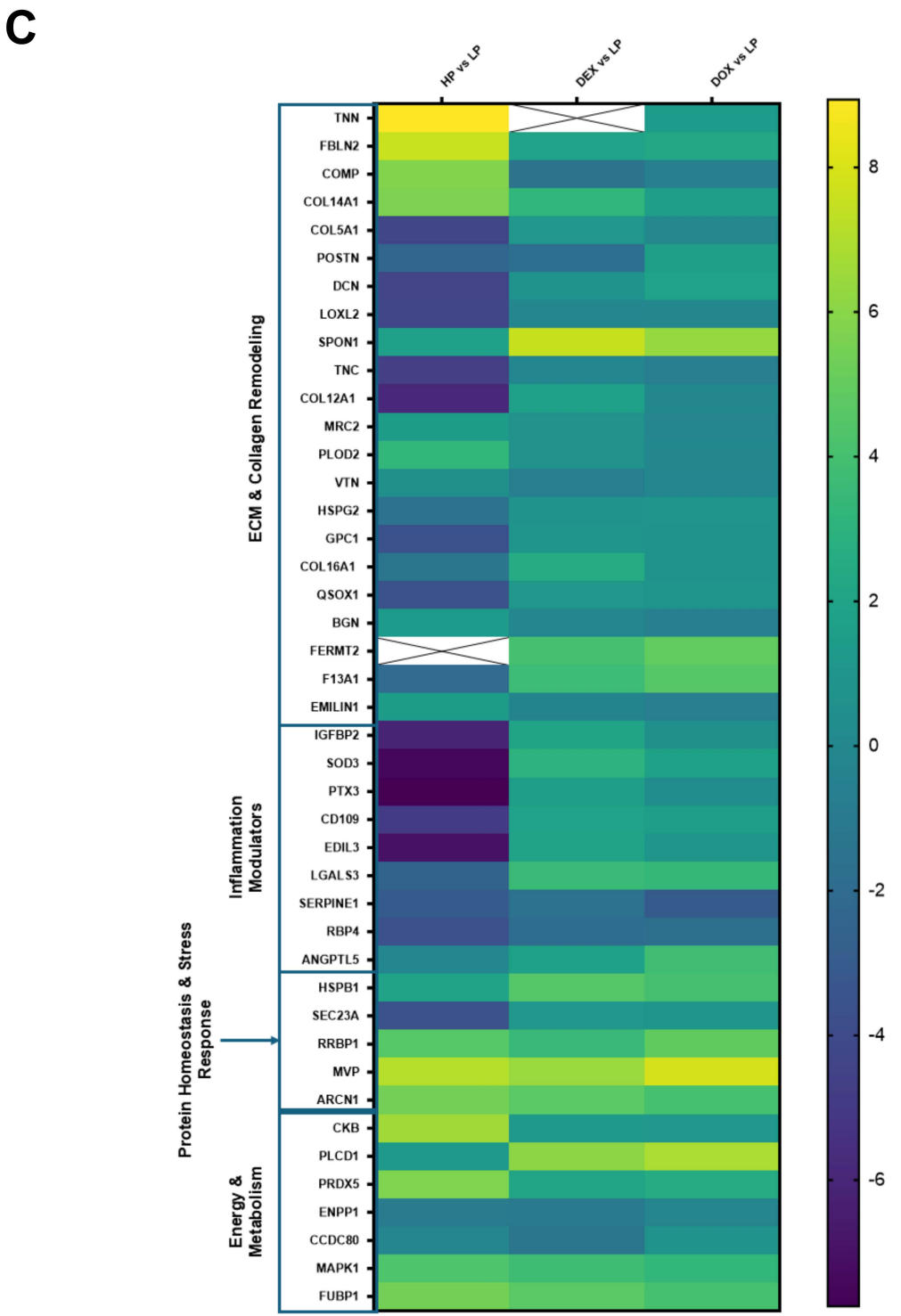
C
HP vs LP
DEX vs LP
DOX vs LP
ECM & Collagen Remodeling
TNN
FBLN2
COMP
COL14A1
COL5A1
POSTN
DCN
LOXL2
SPON1
TNC
COL12A1
MRC2
PLOD2
VTN
HSPG2
GPC1
COL16A1
QSOX1
BGN
FERMT2
F13A1
EMILIN1
Inflammation Modulators
IGFBP2
SOD3
PTX3
CD109
EDIL3
LGALS3
SERPINE1
RBP4
ANGPTL5
Protein Homeostasis & Stress Response
HSPB1
SEC23A
RRBP1
MVP
ARCN1
Energy & Metabolism
CKB
PLCD1
PRDX5
ENPP1
CCDC80
MAPK1
FUBP1
8
6
4
2
0
-2
-4
-6